Model for current patterns in physical systems with two charge carriers

C. Radehaus,* R. Dohmen, H. Willebrand, and F.-J. Niedernostheide
Institut für Angewandte Physik, Universität Münster, 4400 Münster, Federal Republic of Germany
(Received 2 February 1990; revised manuscript received 23 July 1990)

The temporal and spatial evolution of patterns in physical systems due to electrical current flow can be described for a certain class of systems, which includes certain semiconductor and gas discharge systems, by a two-layer model in terms of the electrical current density and the electrical potential. An equation for the nonlinear layer is derived, the characteristic parameters of which can be obtained from experiments at the respective systems without inhomogeneous patterns lateral to the main current direction. The resulting equation takes into account diffusion and drift effects in the nonlinear layer. It turns out that the drift effects occur only if there is a "net space charge." Two special cases are derived depending on which of the two layers gives the main contribution to the displacement current density, and the typical static and dynamic behavior is studied by numerical calculations. Furthermore, the application of the model to real devices is discussed, and a comparison is made with experimental results obtained with a dc glow-discharge system.

I. INTRODUCTION

The formation of temporal-spatial patterns in thermodynamic open systems is a well-known phenomenon.[1] The appearance of inhomogeneous patterns is observed, e.g., in chemistry[2–4] and biology.[5,6] Mathematical investigations were carried out, e.g., by Rothe and Maginu.[7,8] It has been shown in recent studies that such phenomena can also occur in physical systems.[9–11] Special examples for such systems are dc gas-discharge systems,[12–15] semiconductor systems,[16–23] and electrical networks.[11,24–26]

In electrical systems that show different electrical properties along the current direction, often pattern formation lateral to the main current direction is observed. In order to describe such a system it may be possible to divide the system approximately into two layers. In Ref. 16 we have proposed such a two-layer model to describe pattern formation. One of the two layers has linear Ohmic electrical properties, the other one has a nonlinear current controlled current-voltage characteristic, which contains a current region of negative differential resistivity. This model leads to a pair of coupled reaction diffusion equations in terms of the electrical current density and the electrical potential at the interface of the layers. While the equation concerning the linear layer was derived by means of an approximation of the potential, for the nonlinear layer a phenomenological estimate was made that considers diffusion and the reaction of charge carriers. The resulting model realizes the chemical-biological principle of autocatalysis and lateral inhibition[6] and shows interesting dynamic and static patterns. This includes stable spatial patterns, nervelike pulse transmission, or irregular behavior. The same model is obtained when we consider an appropriate electrical network as an equivalent circuit for the two-layer model[24] and carry out the formal limit to the continuous case.

In this work an equation for the nonlinear layer is derived. This is based upon the continuity equation, the Poisson equation, and the usual transport equation for the case of two kinds of charge carriers, which is a fairly weak requirement. By reasonable assumptions for the material and by applying an averaging procedure to the nonlinear region a nonlinear equation is obtained, which has the structure of an ambipolar transport equation that takes into account reaction, diffusion, and drift effects of charge carriers. It turns out that the phenomenological estimate used in Ref. 16 is a special case of this equation. Coupling the nonlinear and the resistivity layers leads to the complete model in terms of a partial current density and potential, both deviating with respect to a reference state.

The outline of the paper is as follows. In Sec. II the equation for the behavior of the partial current density caused by the kinetics of charge carriers in the nonlinear layer is derived, and the complete model is established. Additionally, the stability limits concerning hard- and soft-mode instabilities are given for the purpose of a later discussion of the numerical results. In Sec. III numerical results are presented and ambipolar drift effects are discussed. Furthermore, numerical results concerning irregular dynamic behavior of the system are illustrated by the time dependence of the total current. In Sec. IV the application of the model to real devices is discussed. Especially experimental results of a dc gas-discharge system are shown and compared with the predictions of the extended model. Finally, in Sec. V some conclusions are drawn.

II. DERIVATION OF THE MODEL

The starting point is the physical model of Ref. 16 shown in Fig. 1. It forms a stack of two layers, the linear resistivity layer, labeled L, of thickness b and the nonlinear layer, labeled N, of thickness $a \ll b$. The whole device is enclosed by metal contacts. Applying an external voltage to the metal contacts via the load resistance R_S,

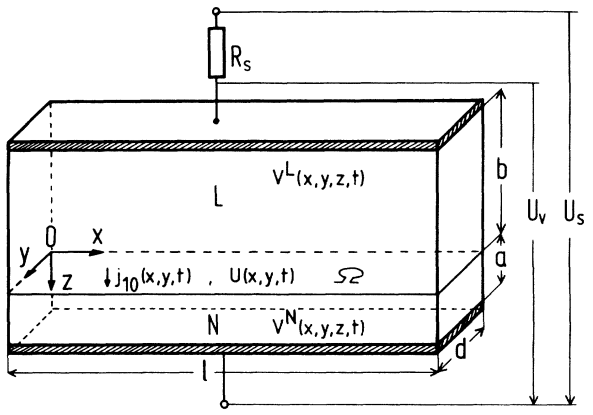

FIG. 1. Physical two-layer model consisting of a resistive layer denoted by L and a nonlinear layer denoted by N; the hatched areas are metal electrodes.

the main current flow direction will be parallel to the z direction. To describe pattern formation in the device we derive a system of equations in terms of deviations of the potential and a partial current density j_{10} relative to a reference state at the interface Ω. j_{10} is the partial z component of the current density due to charge-carrier density deviations from the reference state, from which the total z component of the current density can be computed.

We first derive a nonlinear partial differential equation which should suffice to describe the essential features of the z component of the current density in the layer N caused by a given potential at the interface. Later on this equation will be coupled to an equation for the potential of the linear layer, which has been developed in Ref. 16. The derivation for the equation of the nonlinear layer is carried out for materials in which the kinetics is determined by two kinds of charge carriers. This situation is given, e.g., in certain gas-discharge and semiconductor devices.

In order to simplify the derivation we assume $l \gg d$, i.e., we regard the interface as quasi-one-dimensional. To keep the formulas simple we introduce one-dimensional "current densities" and two-dimensional carrier densities with the units A/m and $1/m^2$, respectively. The derivation can be extended easily to the two-dimensional case.

A. Modeling the nonlinear layer

Owing to the electric field in the nonlinear layer, caused by the electrical potential at the interface, complex transport processes take place accompanied by a typical distribution of electric field, charge carriers, space charges, etc. In order to derive an equation for these complex transport processes we start with the continuity equations for the positive and negative charge carriers of the concentration $n^-(x,z,t)$ and $n^+(x,z,t)$, respectively, and with the Poisson equation. The equations are given by

$$\frac{\partial n^-}{\partial t} = f(n^-,n^+,|\mathbf{E}|)+(1/e)\nabla_{xz}\cdot\mathbf{j}^- ,$$
$$\frac{\partial n^+}{\partial t} = f(n^-,n^+,|\mathbf{E}|)-(1/e)\nabla_{xz}\cdot\mathbf{j}^+ , \tag{1a}$$

$$\nabla_{xz}\cdot\mathbf{E} = (e/\epsilon\epsilon_0)(n^+ - n^- + C) , \tag{1b}$$

where ϵ is the relative dielectric contant and $\epsilon = 8.85\times10^{-12}$ F/m, $\mathbf{E}(x,z,t)$ is the electric field vector, e is the elementary charge, $\nabla_{xz} = (\partial/\partial x, \partial/\partial z)$ and $\Delta_z = \partial^2/\partial z^2$. These equations shall be solved in the region $\Omega\times[0,a]$ with the boundary condition $\int_0^a E_z dz = U$ between the bottom electrode and the interface, and conditions depending on the system at the boundary $\partial\Omega\times[0,a]$ (see Fig. 1). f denotes the reaction term and contains the generation and recombination rates of charge carriers. C is a background charge, which is temporally constant, i.e., $\partial C/\partial t = 0$, and homogeneous in the x direction. The net current density $\mathbf{j}(x,z,t)$ is given by $\mathbf{j} = \mathbf{j}^- + \mathbf{j}^+$ and includes all the contributions of free charge carriers in different states (energy, velocity, etc.). We consider the case that $\mathbf{j}$ can be expressed in the form of the usual transport equations (Refs. 27 and 28 for semiconductors, Ref. 29 for gas discharges)

$$\mathbf{j}^- = en^-\mu^-\mathbf{E} + eD^-\nabla_{xz}n^- ,$$
$$\mathbf{j}^+ = en^+\mu^+\mathbf{E} - eD^+\nabla_{xz}n^+ , \tag{1c}$$

with mobilities μ^+ and μ^- and diffusion constants D^+ and D^- for the positive and negative charge carriers, respectively. Effects caused by temperature and magnetic fields are not taken into account explicitly. To include anisotropic effects which occur, e.g., in semiconductors we choose anisotropic mobilities and diffusion coefficients so that μ^-,μ^+ and D^-,D^+ are diagonal matrices.

The matter of interest in this paper is the time-spatial pattern formation transverse to the main current flow. The description of the inhomogeneous patterns starts from a reference state, which represents a certain configuration of the electric field, the velocity field, and the charge-carrier densities, and is homogeneous in the x direction with an arbitrary structure in the z direction, which is typical for the considered system. Structures in the x direction for given potential in the boundary layer are interpreted as x- and z-dependent deviations from the reference state. Later on, as a result of an averaging procedure, the reference state will supply ambipolar values for the diffusion constant and the mobility of the charge carriers, which are assumed to hold also for a certain vicinity of the reference state. It will turn out that by this averaging procedure the complex processes of pattern formation in the z direction can be established in the parameters (diffusion constant and mobility) as well as in the global $j(U)$ characteristic, which can be obtained easily by experimental measurements. This is a very comfortable way to take account of the influence that these effects in the z direction have on the pattern formation in the x direction. In order to describe the behavior of the nonlinear layer from this viewpoint we set up the following definitions and assumptions.

(i) The stationary reference state, which is homogeneous in the x direction, is given by

$$P_0(z)=(n_0^-(z),n_0^+(z),\mathbf{E}_0(z)) \ . \tag{2a}$$

In this reference state all physical quantities (potential, current flow, etc.) are constants parallel to the electrodes. For illustration the distributions of the electron concentration for a reference state and for an idealized inhomogeneous pattern are shown schematically in Fig. 2.

The stationary reference state P_0 Eq. (2a) satisfies Eqs. (1). From this we obtain

$$-f(n_0^-,n_0^+,|\mathbf{E}_0|)=\mu_{0z}^-\frac{\partial}{\partial z}(n_0^-E_{0z})+\frac{\partial}{\partial z}\left[D_{0z}^-\frac{\partial}{\partial z}n_0^-\right],$$

$$-f(n_0^-,n_0^+,|\mathbf{E}_0|)=-\mu_{0z}^+\frac{\partial}{\partial z}(n_0^+E_{0z})+\frac{\partial}{\partial z}\left[D_{0z}^+\frac{\partial}{\partial z}n_0^+\right], \tag{2b}$$

$$E_{0z,z}=(e/\epsilon_0)(n_0^+-n_0^-+C) \ ,$$

for the given electrical potential $\int_0^a E_{0z}dz=U_0$ at the interface Ω. Expressing n^+, n^-, and $\mathbf{E}$ by deviations

$$(n_1^-(x,z),n_1^+(x,z),\mathbf{E}_1(x,z)) \tag{2c}$$

from the reference state P_0 Eq. (2a), we write these and the additionally listed quantities as sums according to

$$\begin{aligned} &n^+=n_0^++n_1^+, \quad n^-=n_0^-+n_1^- \ , \\ &\mathbf{E}=\mathbf{E}_0+\mathbf{E}_1, \quad U=U_0+U_1 \ , \\ &\mathbf{v}^-=\mathbf{v}_0^-+\mathbf{v}_1^-=-\mu^-(\mathbf{E}_0+\mathbf{E}_1) \ , \\ &\mathbf{v}^+=\mathbf{v}_0^++\mathbf{v}_1^+=\mu^+(\mathbf{E}_0+\mathbf{E}_1) \ . \end{aligned} \tag{2d}$$

$\mathbf{v}^-$ and $\mathbf{v}^+$ are the drift velocities of the charge carriers.

(ii) The deviations of the charge carrier densities from the reference state are supposed to be quasineutral, i.e., $n_1^-=n_1^+$. This means the space-charge distribution of the reference state is constant regardless of the patterns in the x direction.

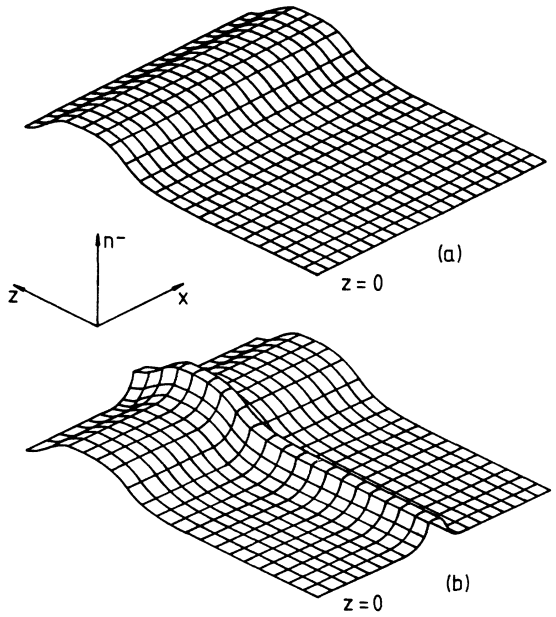

FIG. 2. Schematic illustration of the distribution of an electron concentration for (a) a reference state and (b) an idealized inhomogeneous deviation.

(iii) It is assumed that the mobilities and the diffusion matrices are constant and given by

$$\begin{aligned} D^-&=\begin{pmatrix} D_x^- & 0 \\ 0 & D_z^- \end{pmatrix}, \quad D^+=\begin{pmatrix} D_x^+ & 0 \\ 0 & D_z^+ \end{pmatrix} , \\ \mu^-&=\begin{pmatrix} \mu_x^- & 0 \\ 0 & \mu_z^- \end{pmatrix}, \quad \mu^+=\begin{pmatrix} \mu_x^+ & 0 \\ 0 & \mu_z^+ \end{pmatrix} , \end{aligned} \tag{2e}$$

with

$$\mu_m^+=\alpha\mu_m^-, \quad m=x,z \ . \tag{2f}$$

(iv) The deviations of the quantities (2c) from their averaged values in the z direction are supposed to be small. Furthermore, we restrict the discussion to sufficiently small deviations from the reference state P_0, especially we assume $|\mathbf{E}_1| \ll |\mathbf{E}_0|$.

The last assumptions effect, in particular, $|\mathbf{E}| \approx E_z$, so that the kinetics is determined by E_z. By inserting (1c) and (2e) in (1) we write more explicitly

$$n_{,t}^-=f(n^-,n^+,E_z)+\mu_x^-n_{,x}^-E_x+\mu_x^-n^-E_{x,x}+\mu_z^-n_{,z}^-E_z$$

$$+\mu_z^-n^-E_{z,z}+D_x^-n_{,xx}^-+D_z^-n_{,zz}^- \tag{3}$$

with the notation $n_{,z}\equiv\partial n/\partial z$ for partial derivations, which is used throughout this paper. For the positive charge carriers we get an analogous equation. If we multiply the two equations with appropriate factors, add them, and take advantage of the quasineutrality $n_1^-=n_1^+=n_1$, we get one equation

$$n_{1,t}=G_0^*(n_1,E_{1z})+\mu_0^*n_{1,x}E_{1x}+D_0^*n_{1,xx} \ , \tag{4}$$

with

$$\mu_0^*=\frac{\mu_x^+\mu_x^-(n_0^+-n_0^-)}{\mu_x^+n_0^++\mu_x^-n_0^-}, \quad D_0^*=\frac{\mu_x^+D_x^-n_0^++D_x^+\mu_x^-n_0^-}{\mu_x^+n_0^++\mu_x^-n_0^-}$$

in terms of the deviation n_1 alone. Note that space-charge terms proportional to $E_{1x,x}$ are dropped out by this procedure. G_0^* is an effective reaction term; for details see Appendix A, Eq. (A2b).

Up to now we have succeeded in reducing the behavior of the nonlinear layer to one equation for the special case of two kinds of charge carriers, which behave quasineutrally. The following derivation, however, depends only on an equation of the form (4) and not on how it was obtained. More generally, we can proceed in the same way whenever it is possible to describe the complex behavior of the nonlinear layer with one equation for a physical quantity, which is related to the charge-carrier distributions.

As we want to derive a model in terms of the current density, we use the fact that the current through the system is dominated by the drift current due to the strong electric field in the z direction and consider the z component j_z of the drift current density

$$j_z = j_z^- + j_z^+ = -en^- v_z^- + en^+ v_z^+ = j_0 + j_{Nz} , \quad (5)$$

with j_{Nz} the deviation of the total current density from the reference state. The next aim is to obtain an equation for the evolution of the current density $j_{10} = -e(1+\alpha)n_1 \mu_z^- E_{0z}$, which corresponds to that part of j_{Nz} which takes account only of the changes of charge-carrier concentrations providing a constant velocity field [for details see Appendix A, Eq. (A3)]. In order to set up the evolution equation for j_{10} we multiply Eq. (4) by $-e(1+\alpha)v_{0z}^-$. Because of the constancy of v_{0z}^- in the x direction, we get [for details see (A4)]

$$j_{10,t} = G_0(j_{10}, E_{1z}) + \mu_0^* j_{10,x} E_{1x} + D_0^* j_{10,xx} . \quad (6)$$

This equation is a partial-differential equation for j_{10} of the independent variables x, z, and t with the reference state P_0 as a parameter, as well as E_{1x} and E_{1z} as input parameters. The new "reaction term" $G_0(j_{10}, E_{1z})$ is an operator on j_{10} and E_{1z} because it contains z derivatives. Equation (6) has the structure of an ambipolar diffusion equation for j_{10} and contains a drift term with the effective mobility μ_0^* and a diffusion term with the effective diffusion constant D_0^*.

As we focus our interest on pattern formation in the x direction, whereas the structures in the z direction are not of concern for the present investigation, we eliminate the z dependences by averaging Eq. (6) with respect to z. The averaging is denoted by

$$\langle\ \rangle = (1/a)\int_0^a dz . \quad (7)$$

Each quantity is split up into an averaged value and a deviation. Note that we have deviations from the reference state and deviations from the averaged distribution in the z direction, which should not be confused.

We now want to show under which conditions it is possible to express the averaged equation (6) and especially the reaction term $\langle G_0 \rangle$ in terms of $\langle j_{10} \rangle$ and $\langle E_{1z} \rangle$. For this purpose we carry out a functional expansion of G_0,

$$G_0(j_{10}, E_{1z}) = G_j j_{10} + G_E E_{1z} + G_{jE} j_{10} E_{1z} + G_{jj} j_{10}^2 + G_{EE} E_{1z}^2 + \cdots , \quad (8)$$

around the reference state P_0 with the variational derivatives G_j and G_E, etc. taken at the reference state P_0 and $G_0(0,0)=0$ (see Appendix A) and get

$$\langle j_{10} \rangle_{,t} = \langle G_0 \rangle(\langle j_{10} \rangle, \langle E_{1z} \rangle) + \langle \mu_0^* \rangle \langle j_{10} \rangle_{,x} \langle E_{1x} \rangle + \langle D_0^* \rangle \langle j_{10} \rangle_{,xx} + R_m . \quad (9)$$

R_m contains all higher-order terms of the deviations; for details see Appendix B. In the special case that j_{10} and E_1 are approximately constant in the z direction, the term R_m can be neglected for arbitrary deviations of the functional derivatives and of the constants μ_0^* and D_0^* from their averaged values. For R_m sufficiently small the averaged reaction term $\langle G_0 \rangle$ can be expressed in terms of $\langle j_{10} \rangle$ and $\langle E_{1z} \rangle$ and has the same Taylor-series expansion structure as G_0, but with averaged coefficients.

If there are highly different time scales for different regions along the z axis, the fast time scales are thought to be adiabatically eliminated, and the averaging procedure is then carried out with respect to the remaining region in the z direction. The resulting time constant, which follows from the averaging procedure, is shifted to the larger time scales, which dominate the stability.

Next we determine $\langle E_{1z} \rangle$ and $\langle E_{1x} \rangle$ from the potential distribution at the interface. With $U(x) = U_0 + U_1(x)$ as the electrical potential distribution at the interface, the relation

$$\langle E_{1z} \rangle = U_1(x)/a \quad (10a)$$

holds. In order to compute $\langle E_{1x} \rangle$ we assume that the deviation $V_1(x,z)$ of the potential in the nonlinear layer can be separated into two factors according to $V_1 = U_1(x)\chi_1(z)$ with $\chi_1(0)=1$ and $\chi_1(a)=0$. This estimate holds for small a. it follows that

$$E_{1x} = -\frac{\partial V_1}{\partial x} = -\chi_1(z)\frac{\partial U_1}{\partial x} ,$$

and averaging this we get

$$\langle E_{1x} \rangle = -U_{1,x}\langle \chi_1(z) \rangle . \quad (10b)$$

This means $\langle E_{1x} \rangle$ is proportional to $U_{1,x}$. In Ref. 16 the case $\chi_1(z) = 1 - z/a$ is considered, which leads to $\langle \chi_1(z) \rangle = \frac{1}{2}$. Introducing the notations

$$D_0 = \langle D_0^* \rangle, \quad \mu_0 = \langle \mu_0^* \rangle / \langle \chi_1(z) \rangle, \quad g_0 = \langle G_0 \rangle , \quad (10c)$$

and neglecting the terms R_m resulting from the averaging procedure according to the smallness of the variations from the averaged state, we end up from Eq. (9) with the following equation:

$$\langle j_{10} \rangle_{,t} = D_0 \langle j_{10} \rangle_{,xx} - \mu_0 \langle j_{10} \rangle_{,x} U_{1,x} + g_0(\langle j_{10} \rangle, U_1) . \quad (11a)$$

This equation has the structure of an ambipolar evolution equation for the mean current density $\langle j_{10} \rangle$ depending on the voltage deviation U_1. Besides the "reaction term" g_0, ambipolar diffusion and drift effects are taken into account.

According to Eqs. (10c), (A2a) and (A2b) μ_0 (the coefficient of the drift term) is proportional to $n_0^+ - n_0^-$. If the reference state has no "net charge," the drift term vanishes. In this case, we obtain an equation for the current density $\langle j_{10} \rangle$, which is of the same form as the equation for the nonlinear layer N introduced in Ref. 16. In the following, for the reaction term g_0, we use nonlinear functions of the form

$$g_0(\langle j_{10} \rangle, U_1) = [U_1 - h(\langle j_{10} \rangle)]/\ell \quad (11b)$$

with ℓ as a distributed inductance. By $\langle j_{10} \rangle$ we are able to determine the mean value for the z component of the complete current-density deviation as

$$\langle j_{Nz}\rangle=\langle j_{10}\rangle+\langle a_0\rangle U_1/a+\langle j_{10}\rangle U_1/U_0\ , \tag{11c}$$

by averaging j_{Nz} from (A3) with the same assumptions as used above, where $a_0=j_0/E_{0z}$ denotes the conductivity in the reference state.

Let us briefly discuss what we have done up to now. Initially the description of the nonlinear layer was equivalent with solving a problem in three dimensions. The quasi-one-dimensional consideration ($l\gg d$) meant a reduction to two dimensions, resulting in a system of equations depending on x and z. The solution in the z direction was substituted by measuring the global $j(U)$ characteristic, which is mathematically reflected in the averaging procedure. What is left is an equation describing the pattern formation in the x direction, which takes account of the structures in the z direction only in the form of constant parameters and the $j(U)$ characteristic, which can be obtained from experiments.

B. Modeling the resistivity layer—the complete model

Up to now we have established equations for the physical quantities in the nonlinear layer N. In order to get the complete two-layer model we have to put together the linear and nonlinear layer. To distinguish between physical quantities like current density and electric field in the two layers we denote quantities in the linear resistivity layer with the index "L" and quantities in the nonlinear layer with "N." In the layer N all quantities like the electric field and the current density are averaged in the z direction. In order to get a simple notation in the following, we omit brackets indicating averaging of quantities in the N layer and also omit the index "1" indicating deviations from the reference state P_0. In this way U, U_v, U_s, $I^{\rm tot}$, j and E_{Lz} denote deviations and, e.g., $E_{Nz}\equiv E_{1z}$ means the averaged deviation of the z component of the electrical field in the N layer.

In order to derive a model for the layer L with respect to the potential distribution U at the interface, we use the potential approximation of Ref. 16, which is given by

$$V_L(x,z,t)=U+(U-U_v)z/b-(q_1z+q_2z^2+q_3z^3)U_{,xx}\ , \quad -b<z<0\ . \tag{12a}$$

$$q_1=5b/26,\quad q_2=\tfrac{1}{2},\quad q_3=4/13b\ ,$$

with

$$U_v=U+U_L=U_S-I^{\rm tot}R_S\ , \tag{12b}$$

where R_S is the external load resistance. $I^{\rm tot}$ is given by

$$I^{\rm tot}(t)=\int_0^l j_z^{\rm tot}dx\ , \tag{12c}$$

where $j^{\rm tot}$ is the total current density including the displacement current densities. Its z component is defined as

$$[j_{\rm tot}(x,z,t)]_z=\begin{cases}[j_L^{\rm tot}(x,z,t)]_z=E_{Lz}/\rho+\epsilon_0\epsilon_L E_{Lz,t} \\ \quad \text{for } -b<z<0 \\ [j_N^{\rm tot}(x,z,t)]_z=j_{Nz}+\epsilon_0\epsilon_N E_{Nz,t} \\ \quad \text{for } 0<z<a\end{cases} \tag{13a}$$

where ρ is the specific resistivity of the linear material, and ϵ_0, ϵ_L and ϵ_N are the dielectric constant and the relative dielectric constants, respectively.

In connecting both layers, we must maintain the continuity conditions for the electric potential and for the z component of the total current densities at the interface Ω:

$$[j_L^{\rm tot}(x,z=0,t)]_z=[j_N^{\rm tot}(x,z=0,t)]_z\ .$$

The insertion of (13a) yields

$$\left[\epsilon_0\epsilon_L\frac{\partial}{\partial t}+\frac{1}{\rho}\right]E_{Lz}(x,0,t)=j_{Nz}+\epsilon_0\epsilon_N\frac{\partial E_{Nz}(x,0,t)}{\partial t}\ . \tag{13b}$$

From the potential estimates (12a) and (12b) we can compute E_{Lz} at the interface Ω as

$$E_{Lz}(x,z=0,t)=-\left.\frac{\partial V_L}{\partial z}\right|_{z=0}=\frac{U_v-U}{b}+\frac{5b}{26}U_{,xx}=\frac{U_L}{b}-\frac{5b}{26}U_{L,xx}\ . \tag{14}$$

Now we proceed with Eq. (13b) and insert E_{Lz} from Eq. (14). E_{Nz} is given by Eq. (10a), which reads in the new notation as $E_{Nz}=U(x)/a$. Furthermore, we replace in Eq. (13b) j_{Nz} according to (11c) by $\langle j_{Nz}\rangle$ and obtain the equation

$$\left[\frac{\epsilon_0\epsilon_L\partial}{\partial t}+\frac{1}{\rho}\right]\left[\frac{U_V-U}{b}+\frac{5b}{26}U_{,xx}\right]=\frac{a_0U}{a}+j_{10}+j_{10}\frac{U}{U_0}+\epsilon_0\epsilon_N\frac{U_{,t}}{a}\ ,$$

which can be rewritten as

$$\left[\frac{\epsilon_0\epsilon_L\partial}{\partial t}+\frac{1}{\rho}\right]\frac{5b}{26}\frac{\partial^2U}{\partial x^2}+\epsilon_0\epsilon_L\frac{\partial}{\partial t}\frac{U_V-U}{b}-\left[\frac{1}{b\rho}+\frac{a_0}{a}\right]U+\frac{U_V}{b\rho}=j_{10}+j_{10}\frac{U}{U_0}+\frac{\epsilon_0\epsilon_N}{a}\frac{\partial U}{\partial t}\ . \tag{15a}$$

This is an equation for the evolution of the potential at the interface for a given j_{10}.

Now we have reduced the description of the complete physical model to a system of two equations at the interface Ω. The system consists of the evolution equation (11a) for the averaged current density j_{10}, with the potential U as input, which now is written in the new notation as

$$j_{10,t}=D_0j_{10,xx}-\mu_0j_{10,x}U_{,x}+g_0(j_{10},U)\ , \tag{15b}$$

and the evolution equation (15a) for the potential U with j_{10} as input.

In the following, the limit cases $\epsilon_L/b\ll\epsilon_N/a$ and $\epsilon_L/b\gg\epsilon_N/a$ are investigated, and the model becomes simplest.

1. The case $\epsilon_L/b \ll \epsilon_N/a$

In this case we neglect the displacement current density of the linear layer and Eq. (15a) becomes

$$\frac{\epsilon_0\epsilon_N}{a}U_{,t}=\frac{5b}{26\rho}U_{,xx}-j_{10}-\left[\frac{1}{\rho b}+\frac{a_0}{a}\right]U+\frac{U_V}{\rho b}-\frac{j_{10}}{U_0}U, \tag{16}$$

and the total current $I^{\rm tot}$ is given by (12c) and (13a),

$$I^{\rm tot}(t)=\int_0^l[j_L^{\rm tot}(x',z=0,t)]_z dx'$$

$$=\int_0^l j_{Lz}dx'=\int_0^l\frac{E_{Lz}}{\rho}dx' .$$

Inserting Eq. (14) for E_{Lz} we get

$$I^{\rm tot}(t)=\frac{1}{\rho}\int_0^l\left[-\frac{U-U_V}{b}+\frac{5b}{26}U_{,xx}\right]dx'$$

$$=-\frac{1}{\rho b}\int_0^l U dx'+\frac{lU_V}{\rho b}+B(U_{,x}) ,$$

with $B(U_{,x})=[5b/(26\rho)][U_{,x}(l)-U_{,x}(0)]=0$ for Neumann or periodic boundary conditions, which are used in the following. Thus by solving this equation with respect to U_V we get together with (12b)

$$U_V=U_S-I^{\rm tot}R_S=\frac{1}{1+R_S l/(b\rho)}$$

$$\times\left[U_S+\frac{R_S}{\rho b}\int_0^l U(x')dx'\right] .$$

Combining this with (16) and (15b) and restricting ourselves to functions of the type (11b) we get

$$j_{10,t}=D_0 j_{10,xx}-\mu_0 j_{10,x}U_{,x}+\frac{U-h(j_{10})}{\ell} , \tag{17a}$$

$$\epsilon_0\epsilon_N\frac{U_{,t}}{a}=\frac{5b}{26\rho}U_{,xx}-j_{10}-\left[\frac{1}{\rho b}+\frac{a_0}{a}\right]U-\frac{1}{U_0}j_{10}U$$

$$+\frac{1/(\rho b)}{1+R_S l/(\rho b)}\left[U_S+\frac{R_S}{\rho b}\int_0^l U(x')dx'\right] \tag{17b}$$

for the complete sytem.

Changing to dimensionless variables, with U^* and j^* as problem-dependent normalization constants, according to

$$v=j_{10}/j^*,\quad w=-U/U^*,\quad j^*/U^*=\chi/b\rho ,$$
$$\xi=x/d_w^{1/2},\quad \tau=(\rho b)/(\chi l)t , \tag{18a}$$

and defining

$$\chi=1+(\rho a_0 b)/a,\quad \vartheta=-U^*/U_0 ,$$
$$d_v=D_0\chi\ell/(\rho b),\quad d_w=\tfrac{5}{26}b^2/\chi,\quad \sigma=d_v/d_w ,$$
$$\mu=26\mu_0\ell\chi^2U^*/(5\rho b^3),\quad \delta=\epsilon_0\epsilon_N b^2\rho^2/(a\chi^2 l) ,$$
$$l'=l/(dw)^{1/2},\quad f(v)=-h(j^*v)/U^* , \tag{18b}$$
$$\kappa=U_S/[(1+r)\chi U^*],\quad r=R_S l/(\rho b) ,$$
$$\nabla=\frac{\partial}{\partial\xi},\quad \Delta=\frac{\partial^2}{\partial\xi^2} ,$$

we obtain as the final equation system

$$\frac{\partial v}{\partial\tau}=\sigma\Delta v+\mu(\nabla v)(\nabla w)+f(v)-w , \tag{19a}$$

$$\delta\frac{\partial w}{\partial\tau}=\Delta w+v(1+\vartheta w)-w-\kappa+\frac{r}{1+r}\frac{1}{\chi l'}\int_0^{l'}w(\xi')d\xi' . \tag{19b}$$

Equation (19b) contains the nonlinear term ϑvw. For $|\mathbf{E}_1|\ll|\mathbf{E}_0|$ it follows that $U/U_0=\vartheta w\ll 1$ so that the term ϑw can be neglected. In this case, except for the drift term, we obtain an equation of the same form as that derived for the network of Ref. 25.

2. The case $\epsilon_L/b \gg \epsilon_N/a$

This case is more complex and will require further assumptions to derive simple equations. In this case we neglect the displacement current density of the nonlinear layer and Eq. (15a) turns to

$$\left[\epsilon_0\epsilon_L\frac{\partial}{\partial t}+\frac{1}{\rho}\right]\left[\frac{U_L}{b}-\frac{5b}{26}U_{L,xx}\right]$$

$$=\frac{a_0}{a}(U_V-U_L)+j_{10}\left[1+\frac{U_V-U_L}{U_0}\right] , \tag{20}$$

with $U_L=U_V-U$, where the voltage U_V between the contacts is given by (12b). To avoid time derivatives in the integral terms we express U_V in terms of U_L and j_{10} and compute $I^{\rm tot}$ in the following way:

$$I^{\rm tot}(t)=\int_0^l j_{Nz}(x',z=0,t)dx'$$

$$=\int_0^l\left[\frac{a_0U}{a}+j_{10}\left[1+\frac{U}{U_0}\right]\right]dx' .$$

Together with Eq. (12b) we obtain for U_V

$$U_V=U_S-R_S\left[\frac{a_0U_V l}{a}-\frac{a_0}{a}\int_0^l U_L dx'\right.$$

$$\left.+\frac{1+U_V}{U_0}\int_0^l j_{10}dx'-\frac{1}{U_0}\int_0^l j_{10}U_L dx'\right] ,$$

and solving with respect to U_V yields

$$U_V=\frac{U_S-R_S\left[\int j_{10}dx'-\frac{a_0}{a}\int U_L dx'-\frac{1}{U_0}\int U_L j_{10}dx'\right]}{1+R_S\left[\frac{a_0 l}{a}+\frac{1}{U_0}\int j_{10}dx'\right]} . \tag{21}$$

Combining the two layers by coupling the evolution equations for j_{10} and U_L, i.e., Eqs. (15b) and (20), respectively, and eliminating U by $U=U_V-U_L$ we get, together with (21), the complete equation system in terms of U_L and j_{10}:

$$j_{10,t}=D_0 j_{10,xx}+\mu_0 j_{10,x}U_{L,x}+[U_V-U_L-h(j_{10})]/\ell , \tag{22a}$$

$$\frac{\epsilon_0\epsilon_L}{b}U_{L,t}-\frac{5\epsilon_0\epsilon_L b}{26}U_{L,xxt} =\frac{5b}{26\rho}U_{L,xx}+j_{10}-\left[\frac{1}{\rho b}+\frac{a_0}{a}\right]U_L +\frac{a_0}{a}U_V+\frac{j_{10}(U_V-U_L)}{U_0} \tag{22b}$$

with U_V from (21).

In order to get an equation comparable to Eq. (17) we again use the fact that $U/U_0=(U_V-U_L)/U_0$ is a small quantity, which gives us reason to neglect the last term of Eq. (22b). Additionally, $a_0=e\mu_z^-(n_0^- -\alpha n_0^+)$, Eq. (A3), is assumed to be a small parameter.

Changing to dimensionless variables, with U_L^* and j^* as problem dependent normalization constants, according to

$$\begin{aligned} &v=j_{10}/j^*,\quad w=U_L/U_L^*,\quad U_L^*/j^*=\rho b ,\\ &\xi=x/d_w^{1/2},\quad \tau=(\rho b/\ell)t , \end{aligned} \tag{23a}$$

and defining

$$\begin{aligned} &d_v=D_0\ell/(\rho b),\quad d_w=\tfrac{5}{26}b^2,\quad \sigma=d_v/d_w ,\\ &\mu=26\mu_0 j^*\ell/(5b^2),\quad \delta=\epsilon_0\epsilon_L b\rho^2/\ell ,\\ &l'=l/(d_w)^{1/2},\quad f(v)=-h(j^*v)/U_L^*,\quad \kappa=U_S/U_L^* ,\\ &r=R_S l/(\rho b),\quad \nabla=\frac{\partial}{\partial\xi},\quad \Delta=\frac{\partial^2}{\partial\xi^2} , \end{aligned} \tag{23b}$$

we obtain the final equation system

$$\frac{\partial v}{\partial\tau}=\sigma\Delta v+\mu(\nabla v)(\nabla w)+f(v)-w+\kappa-\frac{r}{l'}\int_0^{l'}v(\xi')d\xi' , \tag{24a}$$

$$\delta\frac{\partial w}{\partial\tau}-\delta\frac{\partial(\Delta w)}{\partial\tau}=\Delta w+v-w . \tag{24b}$$

In the numerical simulations presented in Sec. III we will consider the case where the term $\delta\partial(\Delta w)/\partial\tau$ is neglected. As seen in Sec. II C, this term has no qualitative influence on the linear stability properties. In Ref. 30 it is also shown that it has no considerable effect on the bifurcation into stationary states. This is a motivation to investigate Eqs. (24a) and (24b) at first without this term.

3. Discussion of the two limit cases

Now we have developed the mathematical description of the two-layer model for two special cases. The derived systems of equations have the structure of a reaction-diffusion system. In terms of biomathematics v can be identified locally as activator, w as inhibitor. Additionally, the load resistance causes a global inhibition; in terms of biomathematics this means limited resources.

The two cases of the model refer to where the main capacity is localized. If the capacity is mainly localized in the linear layer L, we get the case $\epsilon_L/b \gg \epsilon_N/a$. The other case corresponds to a capacity localized in the nonlinear layer N. Both cases effect a global inhibition, which has influence on the time behavior of the systems and is reflected in the mathematical description by different integral terms. For the two limit cases this leads to a different dynamic behavior in the case of $R_S\neq 0$.

As mentioned above [Eq. (11a)], we obtain $\mu_0\sim(n_0^+-n_0^-)$ from Eqs. (A2a), (A2b), and (10c). This implies that drift effects only occur if we have a net space charge caused by the positive and negative charge carriers at the reference state P_0. Because of the ambipolar diffusion process we have differential charge separation at the edges of inhomogeneities of the charge carrier distributions. In the case of a net space charge a part of these separated charges is compensated by the net charge. So the component $E_x=-\partial U/\partial x$ arising from the inhomogeneous potential distribution forms driving forces to the edges. The E_x component has opposite signs at the two edges of a current-density inhomogeneity, so the inhomogeneity is expanded or compressed depending on the sign of the net space charge. If $\mu_0=0$, we get the model of Ref. 16. In this case the systems of Eqs. (19) and (24) can be interpreted intuitively by two equivalent circuits in the form of periodic chains of elements. Each element represents the behavior of the corresponding equation at a discrete point of the quasi-one-dimensional interface Ω. The nonlinear layer is represented by a nonlinear resistance and an inductance, which takes into account the time behavior (for details see Ref. 31). The linear layer is represented by two resistances, one modeling the current flow in the z direction and the other the current flow parallel to the electrodes. In this way the current flow parallel to the electrodes couples adjacent elements. To simulate the displacement current a condenser is placed in parallel to the resistance of the linear layer or to the nonlinear resistance according to the two cases

$\epsilon_L/b \gg \epsilon_N/a$ and $\epsilon_L/b \ll \epsilon_N/a$, respectively. By applying Kirchhoff's rules we obtain the spatially discretized form of the systems of Eqs. (19) and (24), respectively, for a discretization according to Euler. The procedure for obtaining the network equations is described in detail in Ref. 25. The network with a condenser in the nonlinear layer is investigated in Refs. 11 and 24–26; the network with the condenser in the linear layer is introduced in Ref. 30.

4. *Relationship between the characteristic $h(j_{10})$ and the total characteristic $H(j_z)$*

In experiments it is often easier to determine the characteristic $U_0+U=H(j_z)$ instead of $U=h(j_{10})$, where j_z is the whole current density according to definition (5) and j_{10} is the partial current density used in the equations. Here we want to show how to obtain $h(j_{10})$ for the partial current density if $H(j_z)$ is given. At first we fix a reference state P_0, which corresponds to (j_0, U_0) [see (A3)] and define the function H_1 according to

$$U=H_1(j_{Nz})=H(j_0+j_{Nz})-H(j_0) .$$

By solving Eq. (11c) with respect to j_{10} we get

$$j_{10}=\frac{j_{Nz}-(a_0/a)U}{1+U/U_0} , \tag{25}$$

so that it is possible to determine the characteristic that fulfills the condition $H_1(j_{Nz})=U=h(j_{10})$ numerically by computing (j_{10}, U) point by point. For definitions see Appendix A, Eq. (A3). For the case where U/U_0 and a_0 are small parameters the two current densities j_{10} and j_{Nz} and the characteristics H_1 and h coincide. In the neighborhood of this limit case we derive an analytical relationship between the two characteristics. $h(j_{10})$ can be derived from $H_1(j_{Nz})$, with j_{Nz} from Eq. (11c), in the following way:

$$\begin{aligned} h(j_{10}) &= H_1(j_{Nz}) \\ &= H_1(j_{10}+(j_0/U_0)U+(j_{10}/U_0)U), \quad U=h(j_{10}) \\ &= H_1\left[j_{10}+\frac{j_0+j_{10}}{U_0}h(j_{10})\right] \\ &= H_1(j_{10})+H_1' h(j_{10})\frac{j_0+j_{10}}{U_0}+\cdots , \end{aligned}$$

with

$$H_1'=\left.\frac{\partial H_1}{\partial j_{Nz}}\right|_{j_{Nz}=j_{10}} .$$

Restricting ourselves to the first order of the expansion, we can solve with respect to $h(j_{10})$

$$h(j_{10})=\frac{H_1(j_{10})}{1-H_1'(j_0+j_{10})/U_0} . \tag{26}$$

The derivation of $H_1(j_{Nz})$ from $h(j_{10})$ is carried out in a similar way. The limit case $j_{Nz}\approx j_{10}$ means physically that the partial current density $j_{01}=(j_0/E_{0z})E_{Nz}$ is small because the conductivity $j_0/E_{0z}=a_0$ is small. Because of $|j_2|<|j_{01}|$ the partial current density j_2 can also be neglected. In this case the velocity distribution of the charge carriers is approximately constant in the x direction.

C. Linear stability analysis of the system

To get more insight into the system it is useful to investigate the destabilization of the stationary homogeneous solutions of the systems (19) and (24) by considering the eigenvalues of the linearized equations. To obtain the eigenvalues $\omega(k)$ we make the following assumption for the perturbations of v^i and w^i in the homogeneous state (v_s^i, w_s^i):

$$\begin{pmatrix} v^i \\ w^i \end{pmatrix} = \begin{pmatrix} v_k^i \\ w_k^i \end{pmatrix} \varphi^i(k,\xi)\exp[\omega^i(k)\tau] .$$

$i=1,2$ corresponds to the Eqs. (19) and (24), respectively; $\varphi^i(k,\epsilon)$ are the eigenfunctions of the Laplace operator to the eigenvalue $-k^2$ for the interface Ω of Fig. 1 with the given boundary conditions.

This leads to the following matrices of the linearized systems:

$$C_k^1=\begin{pmatrix} -\sigma k^2+f' & -1 \\ 1/\delta & -(1+k^2)/\delta+\delta_{k,0}r/[(r+1)\chi\delta] \end{pmatrix} \tag{27a}$$

for Eq. (19) with $\vartheta=0$ and

$$C_k^2=\begin{pmatrix} -\sigma k^2+f'-r\delta_{k,0} & -1 \\ 1/(\delta+\delta k^2) & -1/\delta \end{pmatrix} \tag{27b}$$

for Eq. (24). Here $f'=\partial f/\partial v$ at v_S and $\delta_{k,1}$ denotes the Kronecker symbol. The integral term is replaced by a term proportional to $\delta_{k,0}$. This is valid for the case of eigenfunctions with vanishing mean value for $k>0$. Equations (27a) and (27b) are independent of μ, the dependence on κ is contained in f', as v_S depends on κ.

If $\mathrm{Re}[\omega^i(k)]$ is negative for all k, the system is linearly stable. This is fulfilled if $\mathrm{Det}(C_k^i)>0$ and $\mathrm{Tr}(C_k^i)<0$ for all k. The stability margins for the hard-mode and the soft-mode instability are given by $\mathrm{Tr}(C_k^i)=0$ and $\mathrm{Det}(C_k^i)=0$, respectively. Solving these functions with respect to f' we get the two neutral curves $f_s'^{\,i}(k)$ and $f_H'^{\,i}(k)$. From Eq. (27a) it follows that

$$\begin{aligned} f_H'^{\,1}(k) &= \begin{cases} (\sigma+1/\delta)k^2+1/\delta & \text{for } k>0 \\ [1-r/\chi(r+1)]/\delta & \text{for } k=0 \end{cases} \\ f_s'^{\,1}(k) &= \begin{cases} \sigma k^2+1/(k^2+1) & \text{for } k>0 \\ \{1-r/[(r+1)\chi]\}^{-1} & \text{for } k=0 \end{cases} \end{aligned} \tag{27c}$$

and from (27b)

$$f_H'^{\,2}(k)=\begin{cases}\sigma k^2+1/\delta & \text{for } k>0\\ 1/\delta+r & \text{for } k=0\end{cases}$$
$$f_S'^{\,2}(k)=\begin{cases}\sigma k^2+1/(1+k^2) & \text{for } k>0\\ 1+r & \text{for } k=0\ .\end{cases} \tag{27d}$$

As mentioned above, the term $\delta\partial(\Delta w)/\partial\tau$ of Eq. (24b) shall be neglected in the numerical simulations. By doing so, the neutral curve $f_H'^{\,2}$ is slightly varied in such a way that the factor of k^2 becomes $\sigma+1/\delta$ [see Fig. 3(b)]. This means the modes $k>0$ will be more stable when neglecting the term $\delta\partial(\Delta w)/\partial\tau$, whereas the neutral curve for the soft-mode instability remains unchanged so that the qualitative behavior is the same as before. This gives us reason to examine the equation without this term.

For a rough impression of the behavior of the system it is useful to discuss the stability properties by means of the neutral curves. For $r=0$ the neutral curves for both systems have no discontinuities at $k=0$. The neutral curve for the hard-mode instability always has a minimum at $k=0$, i.e., the hard-mode instability can take place only for the mode $k=0$, especially if the system cannot be destabilized by traveling waves. For $\sigma<1$ the neutral curve for the soft-mode instability reaches its minimum at $k\neq 0$ depending on the value of σ, i.e., the system can be destabilized by stationary spatially periodic waves. The parameter δ has only an effect on the hard-mode neutral curves f_H'. Large values for δ make the system generally more unstable in such a way that the curves $f_H'^{\,i}$ move downwards, and homogeneous oscillations are preferred.

For $r\neq 0$ discontinuities in the neutral curves occur at $k=0$, and for both systems the value of $f_s'^{\,i}(0)$ becomes larger with respect to the case $r=0$, i.e., the destabilization of the mode $k=0$ becomes less likely. For the mode $k=0$ the two systems differ in the hard-mode instability. In system (19) the critical value $f_H'^{\,1}(0)$ becomes smaller with respect to the case $r=0$, whereas in system (24) the critical value $f_H'^{\,2}(0)$ becomes larger, i.e., the mode $k=0$ is more likely to be destabilized for system (19).

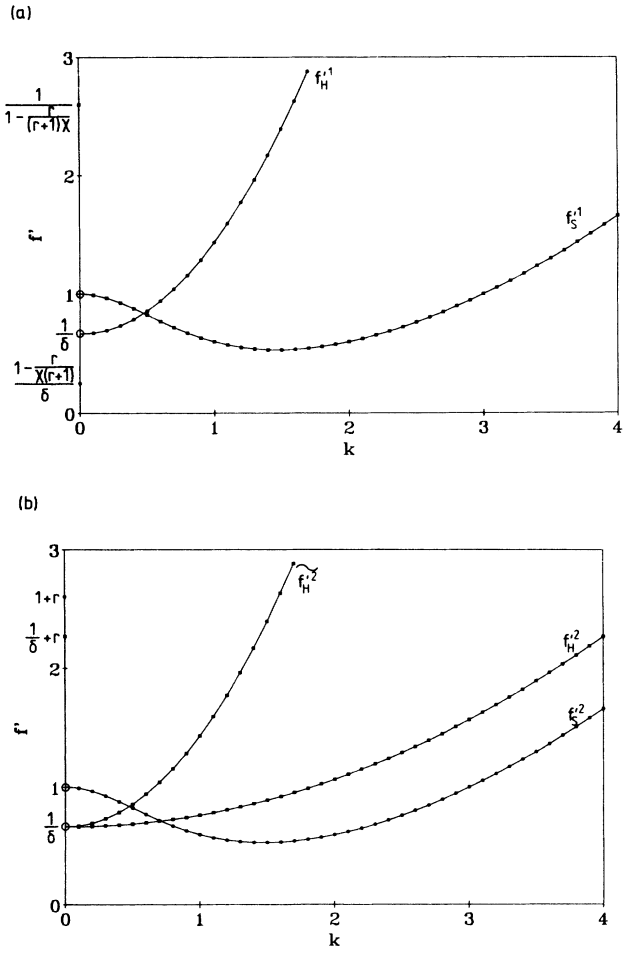

FIG. 3. Examples for the neutral curves of the hard-mode and soft-mode instabilities: (a) $f_H'^{\,1}$ and $f_S'^{\,1}$ corresponding to system (19) with $\vartheta=0$, (b) $f_H'^{\,2}$ and $f_S'^{\,2}$ corresponding to system (24); neglecting the term $\delta\partial(\Delta w)/\partial\tau$, the hard-mode neutral curve changes to $\tilde{f}'_H{}^2$. Parameters in both cases: $\sigma=0.1$, $r=1.6$, $\delta=1.5$, and $\kappa=1.0$.

III. NUMERICAL RESULTS

The equations for the two special cases of Secs. II B 1 and II B 2 show a rich variety of interesting structures. In the following we present typical numerical results concerning the static and dynamic behaviors of the dimensionless equations for one-dimensional space. The two systems are treated numerically in the following form. For the case $\epsilon_L/b \ll \epsilon_N/a$ we restrict ourselves to $\vartheta=0$ and $\chi=1$ with respect to Eqs. (19),

$$\frac{\partial v}{\partial\tau}=\sigma\Delta v+\mu(\nabla v)(\nabla w)+f(v)-w\ , \tag{28a}$$
$$\delta\frac{\partial w}{\partial\tau}=\Delta w+v-w-T\ , \tag{28b}$$

with

$$T=\kappa-\kappa_2 J,\quad \kappa_2=r/(r+1),\quad J=\frac{1}{l'}\int_0^{l'} w(\xi')d\xi'\ .$$

Concerning the second system for the case $\epsilon_L/b \ll \epsilon_B/a$ we neglect the term $\delta\partial(\Delta w)/\partial\tau$ with respect to Eqs. (24). This yields

$$\frac{\partial v}{\partial\tau}=\sigma\Delta v+\mu(\nabla v)(\nabla w)+f(v)-w+T\ , \tag{29a}$$
$$\delta\frac{\partial w}{\partial\tau}=\Delta w+v-w\ , \tag{29b}$$

where

$$T=\kappa-\kappa_2 J,\quad \kappa_2=r,\quad J=\frac{1}{l'}\int_0^{l'} v(\xi')d\xi'\ .$$

In the calculations we approximate the nonlinearity $f(v)$ by a function that is composed of a cubic and a quadratic polynomial. Both are connected continuously differentiable in v_f:

$$f(v)=\begin{cases}\gamma v^3+\lambda v & \text{for } v\le v_f\\ \alpha v^2+\beta v+\theta & \text{for } v>v_f\ ,\end{cases} \tag{30}$$

where

$$v_f=\frac{\alpha}{3\gamma}\left[1+\left[1+\frac{3\gamma(\beta-\lambda)}{\alpha^2}\right]^{1/2}\right],$$

$$\theta=\frac{v_f[2(\lambda-\beta)-\alpha v_f]}{3}$$

for given α, β, γ, and λ. For $v_f\to\infty$ the special case of a cubic polynomial is obtained. Figure 4 shows the isocline system of Eqs. (28) and (29) for the decoupled system and $\kappa_2=0$. Depending on the value of λ in (30), the uncoupled system possesses one or three steady states.

The numerical simulations of Eqs. (28) and (29) have been carried out with homogeneous Neumann boundary conditions. For the calculation of stationary patterns Euler's method was used for differential equations in the explicit and/or implicit form, and the dynamic solutions were calculated by the Crank-Nicholson method. In all cases where different methods were used, the same final results was obtained. The initial conditions for each calculation are mentioned later in the text.

A. Stationary structures

In general small values for the parameter δ in Eqs. (28) and (29) favor stable stationary states as has been discussed in Sec. II C. If additionally σ is small, inhomogeneous stable states are favored because the minimum of the soft-mode neutral curve is shifted to lower values of f' for decreasing σ. The parameter μ does not appear in the linear stability analysis, but may be important when taking into account nonlinear terms.

Near the critical point of the soft-mode instability analytical results can be obtained, which are presented in Ref. 30. In this section the behavior of the system, especially going beyond the range of analytical treatment of Ref. 30, is treated by numerical simulations. These simulations are carried out analogously to experiments by a variation of κ, which corresponds to variations of the externally applied voltage U_s of Fig. 1. In order to get a stable stationary structure we start with the stationary distribution corresponding to the previous value of κ.

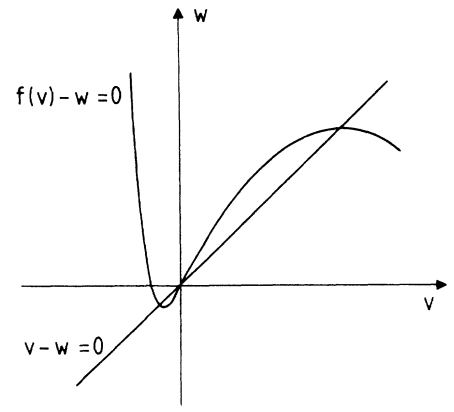

FIG. 4. Isocline system of the spatially decoupled systems (28) and (29) for the case $\kappa=\kappa_2=0$, i.e., $T=0$. For $f(v)$ a function of the form (30) is used. Depending on the model, a value $T\neq 0$ corresponds to a shift of the straight line parallel to the v axis by $-T$ or a shift of the nonlinear characteristic by the value T.

1. $\kappa_2=0$, varying κ

The first case refers to $\kappa_2=0$ due to $R_S=0$; the two special systems (28) and (29) coincide except for a simple transformation of w. This case was roughly sketched in Ref. 16 and now is studied in more detail. We use the cubic nonlinearity $f(v)=\lambda v+\gamma v^3$ in the whole v range and study Eq. (28). By monotonically increasing or decreasing κ over the whole range we vary in Fig. 4 the position and the number of intersection points of the straight line with respect to the nonlinear function $f(v)$. Along with the variation of the intersection points the slope f' at those points is varying and therefore the stability properties are changing. This can be seen from the diagrams f' versus k in Fig. 3.

Carrying out the described simulation for selected values of λ we get the curves of Fig. 5(a) for J versus the term $T=\kappa$, which corresponds to the global I-U_V characteristic of the device of Fig. 1. All numerical simulations in this section are carried out without considering noise unless it is mentioned explicitly. From the diagram in Figs. 5(a) and 5(b) we see that the behavior of the systems depends on the form of the nonlinear function. There exist three characteristic values of λ, for which the behavior of the system changes. Two of them, denoted by λ_1 and λ_2, result from bifurcation analysis.[30] While λ_1 merely depends on σ, λ_2 depends on σ, κ_2, and μ. For $\mu=0$ these values are given by

$$\lambda_1=\sigma^{1/2}(2-\sigma^{1/2}),$$

$$\lambda_2=\lambda_1+\frac{(1-\sigma^{1/2})^2}{(8+30\sigma^{1/2})/9\sigma^{1/2}-Q(\kappa_2)},$$

$$Q(\kappa_2)=\begin{cases}\dfrac{4\kappa_2}{(\sigma^{1/2}-1)^2+\kappa_2} & \text{for system (29)}\\[2ex] \dfrac{4\kappa_2}{(\sigma^{1/2}-1)^2+\kappa_2\lambda_1} & \text{for system (28)}.\end{cases}$$

The third characteristic value, denoted by λ_3, is larger than λ_2, but the exact value could not be determined yet. The typical behavior of the model shall be discussed by means of these characteristic values.

For $\lambda<\lambda_1$ the corresponding distributions for v and w remain homogeneous during one sweep, because the slope f' of the nonlinear characteristic is smaller than the minimum of the soft-mode neutral curve in the whole range.

For $\lambda_1<\lambda<\lambda_2$ the homogeneous state is destabilized when the slope at the operating point is equal to the minimum of the soft-mode neutral curve. This is given when κ reaches the critical value

$$\kappa_{cr}(\lambda)=-\left[\frac{\lambda_1-\lambda}{3\gamma}\right]^{1/2}\left[1-\frac{2\lambda+\lambda_1}{3}\right].$$

At this point the system undergoes a supercritical bifurcation, i.e., it changes continuously into a spatially periodic steady state with growing amplitude by further increasing κ. The amplitude reaches a maximum for $\kappa=0$ and decreases for positive values of κ to a homogeneous distribution at $-\kappa_{cr}$ as can be seen in Fig. 5(c) for $\lambda=0.5$ and the amplitude defined as half of the difference between the maximum and minimum value of v within the distribution. The resulting characteristic J versus κ is continuous without any hysteresis [see Fig. 5(a), curve $\lambda=0.5$].

For $\lambda_2<\lambda<\lambda_3$ the homogeneous state is again destabilized when the critical value κ_{cr} is reached, but jumps discontinuously into a spatially periodic steady state with well-defined wave number k, i.e., the system undergoes a subcritical bifurcation. The amplitude of this state grows up to a maximum and vanishes discontinuously when a second critical value κ'_{cr} is reached, where $|\kappa'_{cr}|>|\kappa_{cr}|$ [see Fig. 5(c), curve $\lambda=0.8$]. Passing through the critical region the other way around we observe a hysteretic behavior of the amplitude curve and of the J-T characteristic. Note that the characteristic is unique at the origin [see Fig. 5(a), curve $\lambda=0.9$ and the larger scale presentation in Fig. 5(b)].

For $\lambda>\lambda_3$ the spatially uncoupled system has three steady states corresponding to two stable and one unstable homogeneous state. When reaching the critical value κ_{cr} the system jumps discontinuously from one homogeneous state into the opposite homogeneous state and the J-T characteristic shows an enlarged hysteretic region, the origin is not unique [see Fig. 5(a), curves $\lambda=2.5,3.0$]. If we apply noise, we can observe as intermediate state an inhomogeneous distribution, which hints that the system is multistable for this parameter range. The distribution reached depends on the history of the system (see Fig. 6).

2. $\kappa_2>0$, varying κ

This case is characterized by an additional global inhibition, which is controlled by the total current flow and leads to a kind of limited resource controlled by the load resistance R_S in the following way. If at a certain location there is a high current flow, the other regions are hindered from switching to a high current state. This leads to a competition of the occurring patterns resulting in localized patterns. We now have to distinguish between the two cases $\epsilon_L/b \ll \epsilon_N/a$ and $\epsilon_L/b \gg \epsilon_N/a$. In the following we present numerical simulations carried out in the same way as has been done for the case $\kappa_2=0$ with a somewhat changed value for λ_2. The main difference is that solitary structures in the form of single filaments and also groups of filaments can occur by the competition. In contrast to the case $\kappa_2=0$, where spatial modulations appear all over the space, we now observe well-defined regions of nearly homogeneous distribution and other regions with strong modulation of v and w.

For $\lambda<\lambda_1$ and $\lambda_1<\lambda<\lambda_2$ we obtain similar results as those observed in the case $R_S=0$.

For $\lambda_2<\lambda<\lambda_3$, the parameter range of the subcritical bifurcation, we get a separation into two spatial regions

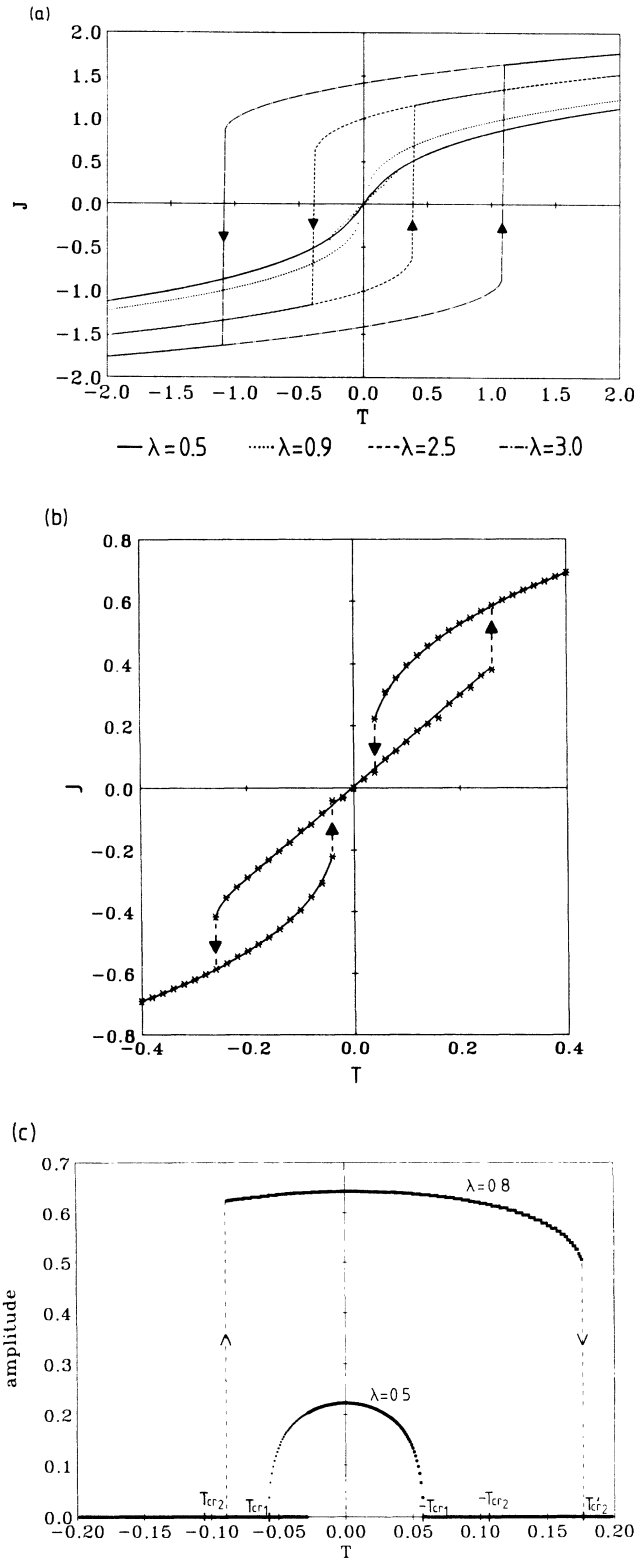

FIG. 5. (a) J-κ characteristic obtained from (29) with $f(v)$ from (30) for selected values of λ. Parameters: $\sigma=0.071$, $\mu=0$, $\gamma=-1$, $\alpha=0$, $\beta=-50$, $\delta=1$, and $r=0$. (b) Larger-scale presentation of the curve $\lambda=0.9$ of (a). (c) Amplitude of v defined by half of the difference of the maximum and minimum values of the v distribution vs $T=\kappa$ for $\lambda_1<\lambda=0.5<\lambda_2$ and $\lambda_2<\lambda=0.8<\lambda_3$, respectively, and the other parameters as in (a).

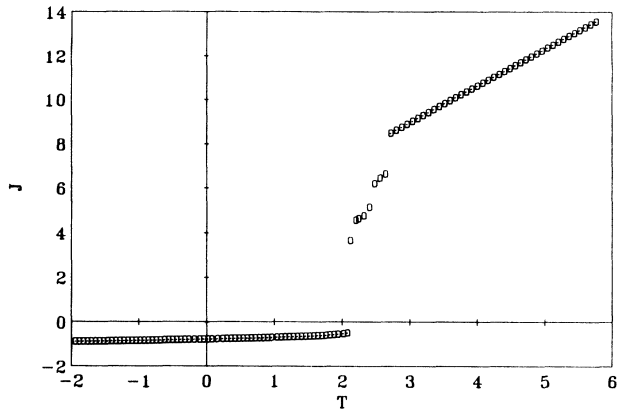

FIG. 6. J-κ characteristic obtained from (29) with $f(v)$ of (30) for $\lambda > \lambda_3$ with (○) and without (●) noise. Parameters: $\lambda = 2.0$ and the other parameters are the same as in Fig. 5.

when reaching the critical value T_{cr}, a homogeneous and a spatially periodic region [see Fig. 7(a)]. Increasing κ the periodic region becomes larger, whereas the homogeneous region is decreased until the whole interface is filled by the periodic pattern. This behavior is accompanied by small discontinuities in the J-T characteristic. By further increasing of κ, the amplitude of the periodic pattern grows, reaches a maximum at $T=0$, and decreases again. When reaching T'_{cr} the structures vanish, accompanied by a steep slope in the J-T characteristic, until the distribution is homogeneous again [see Fig. 7(b)]. By decreasing κ we observe a hysteretic behavior, but as in the case of $R_s = 0$, the J-T characteristic is unique at the origin.

For $\lambda > \lambda_3$ the homogeneous state is again destabilized upon reaching the critical value T_{cr} and bifurcates into a spatially periodic pattern, which, however, is not stable but increases in amplitude. Through this pattern we have a grid of peaks the amplitude of which increases. Now the competition takes effect and through fluctuations one of the peaks is selected and enlarges at the expense of all other peaks resulting in a solitary filament at one of the well-defined maxima of the preceding periodic pattern (winner-takes-all principle).

Up to now the drift term does not affect the solutions qualitatively. However, it becomes important for the process of generation of more filaments. When reaching the critical point at both sides of an existing filament, the distribution of v and w is modulated by a wave, the amplitude of which is very small and strongly decaying with the distance from the filament so that the region appears to be homogeneous in Fig. 8(a). For $\mu = 0$ further filaments are spontaneously generated at the maxima of this modulation accompanied by a discontinuity in the J-T characteristic [see Figs. 8(a) and 8(b)]. In the case of appropriately chosen $\mu \neq 0$, new filaments are generated by the separation of already existing filaments into two. This is also reflected in the shape of the resulting J-T characteristic [see Figs. 9(a) and 9(b)] in that the critical value of T, at which the first filament was generated, is not reached again. These differences will be discussed in detail later on in connection with the experimental results.

B. Nonstationary structures

Large values of the parameter δ favor nonstationary structures, and calculations done so far show that if, in addition, σ is large, nonstationary inhomogeneous patterns may appear. In this case exciting temporal-spatial patterns can be observed. In what follows we present calculations of the dynamic behavior for some typical sets of parameters. The diagrams show the temporal evolution of the spatial patterns and/or time series of the mean current density J. We observe the following typical kinds of behaviors.

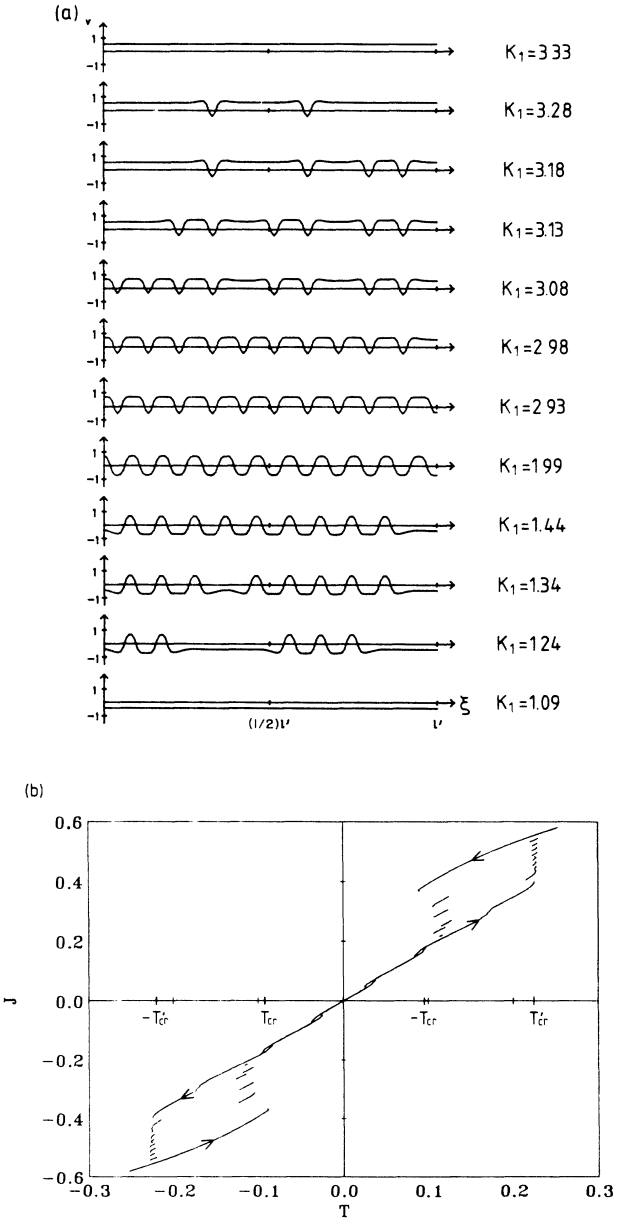

FIG. 7. (a) Spatial distribution of v and (b) J-κ characteristic of system (29) for $\lambda_2 < \lambda < \lambda_3$. Parameters: $\sigma = 0.071$, $\mu = 0$, $\gamma = -1$, $\alpha = 0$, $\beta = -50$, $\delta = 1$, $r = 4$, and $\lambda = 0.9$.

Self-creation and propagation of pulses. To get this behavior we work with no-flux boundary conditions and operate system (29) with $\kappa_2 \neq 0$ and λ around 1 near the threshold where the stationary homogeneous state is destabilized. Starting from a homogeneous initial condition near this critical point and, applying noise, a pulse is created which splits into two pulses that move in opposite directions. When the two pulses have a sufficiently large distance, two new pulses are generated spontaneously between them, while the initial pulses vanish at the boundaries. Figures 10(a) and 10(b) show this behavior of the distribution and the corresponding time series of J.

Oscillating homogeneous domains. Operating system (29) with $r \neq 0$ and a large value of δ, and starting from an initial condition, where about half of the distributions v and w in the center of the system is put in a state of higher concentration, we observe an oscillation of the homogeneous domains as presented in Fig. 11.

Breathing filaments. The breathing filament as presented in Fig. 12 is obtained when the system (28) is operated with the parameters $r=0$, $\lambda \approx 1.4$, and a large

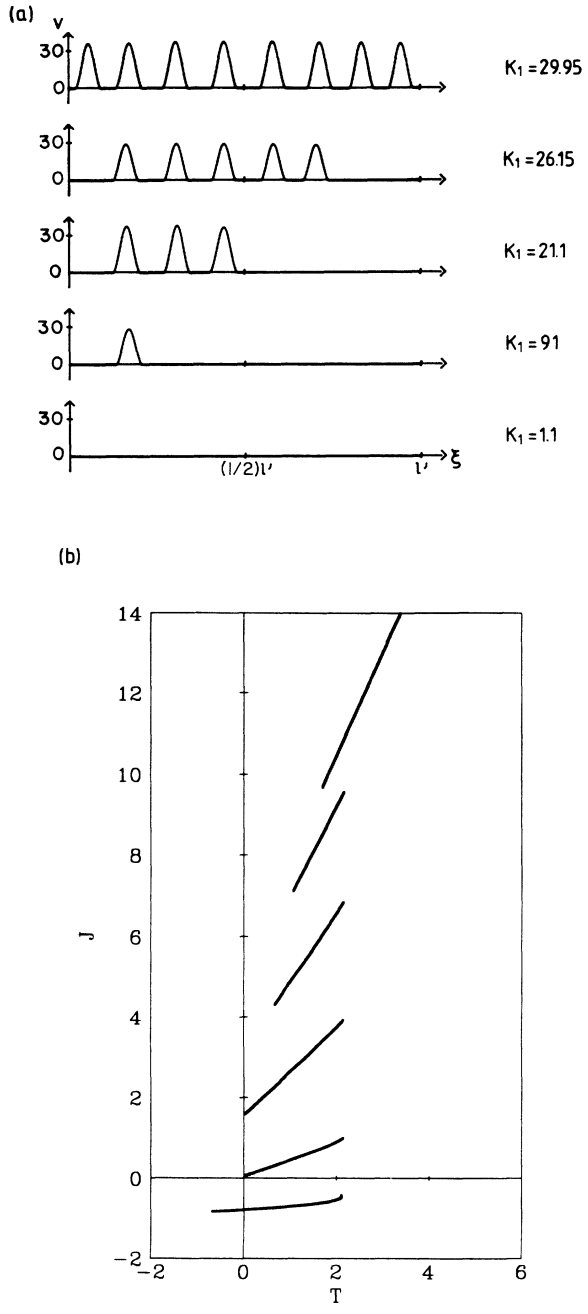

FIG. 8. (a) Spatial distribution of v and (b) J-T characteristic of system (29) by changing κ; the filaments are spontaneously generated from the quasihomogeneous parts of the distribution accompanied by discontinuities in the J-T characteristic. Parameters: $\sigma=0.1$, $\mu=0$, $\gamma=-11.5$, $\lambda=7.89$, $\alpha=0$, $\beta=0.6$, $\delta=1$, and $r=4$.

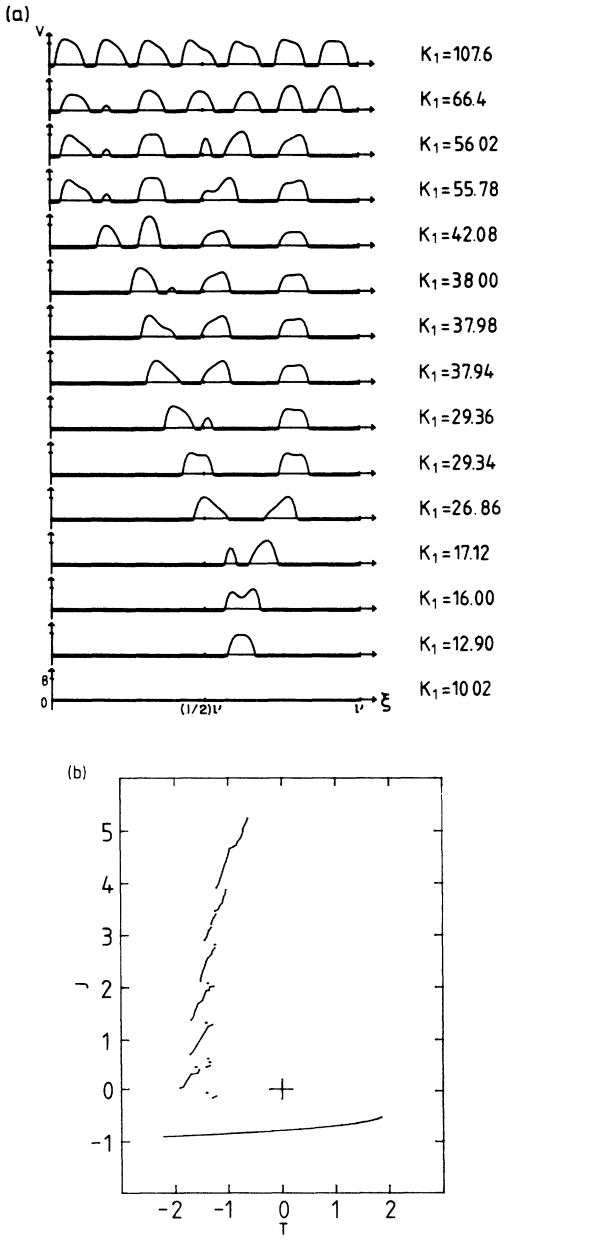

FIG. 9. Analogous simulation to the one in Fig. 8, but with changed parameters, especially $\mu \neq 0$, which causes a division of filaments. Parameters: $\sigma=0.1$, $\mu=0.000035$, $\gamma=-11.5$, $\lambda=7.89$, $\alpha=0$, $\beta=0.6$, $\delta=0.1$, and $r=10$.

value of δ. As an initial condition a distribution for v and w was chosen, about 20% of which was lifted to a higher concentration. This filament becomes alternately thin with a higher amplitude and broad with a somewhat lower amplitude. The time series of the mean current density J is sinusoidal [see Fig. 12(b)]. A similar behavior if predicted in Ref. 28 for a semiconductor model and was also observed by Mimura.[32]

By carrying out a similar numerical simulation with system (29), but choosing two induced filaments as initial condition and $r \neq 0$, we observe an oscillating motion of a "push-pull" mode [see Fig. 13(a)], i.e., when either of the filaments reaches its maximum in width, the other one attains its minimum, and vice versa. The time series of the mean current density J is a sinusoidal signal with a hint of period doubling [see Fig. 13(b)].

Irregular behavior. By increasing μ, for a given set of parameters we can obtain a transition from a stationary structure to a nonstationary irregular behavior. The filaments start to move, then coalesce and split in an irregular way. This is reflected in the time series of the mean total current, which also has an irregular shape. Figure 14 shows the time series of both systems. Note that there is a qualitative difference between the two signals. For system (29) it is mainly the amplitude of the signal that is irregular, while for system (28) the frequency also shows an irregular shape.

By these examples we gave a rough impression of the interesting dynamic behaviors that are obtained when operating the systems with large values of δ and σ. The patterns keep their solitary character, but show nervelike pulse motion, oscillations of the filament walls, and irregular behavior of filaments. There are several authors[34] who consider stationary and nonstationary solutions of equations, which are very similar to the systems under discussion except for the integral term. The results concern mainly the bifurcation into periodic structures, the stability of filaments, and the propagation of nervelike pulses. Some of the papers also report breathing motion.

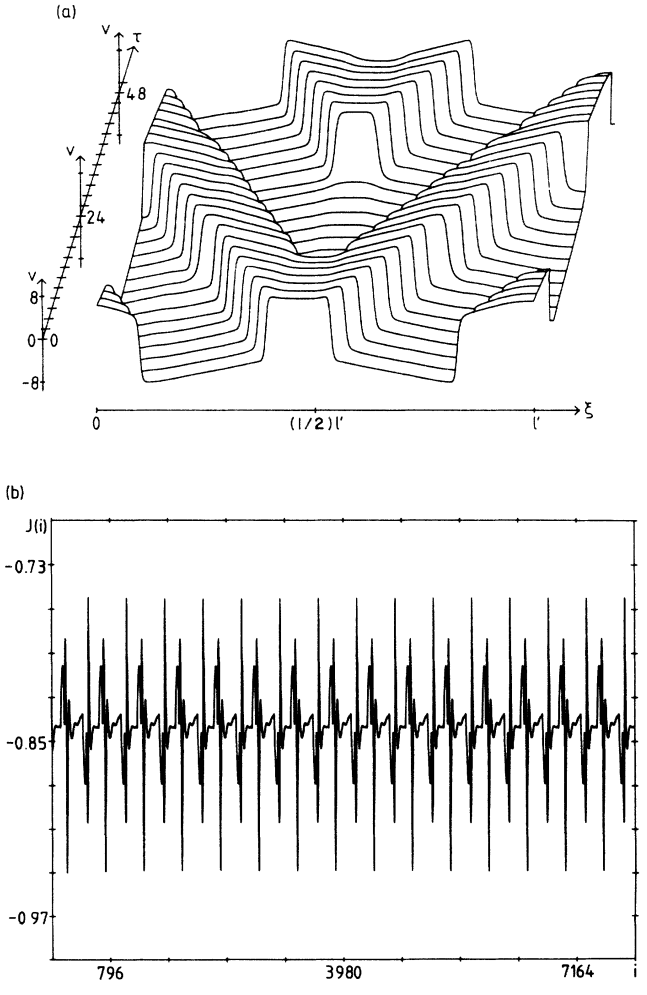

FIG. 10. (a) Time evolution of the spatial distribution of v and (b) time series J vs number i of time steps $\Delta\tau$ in the pulse transmission mode obtained from system (29) with $f(v)$ from (30). Parameters: $\sigma = 100\,000$, $\mu = 0$, $\gamma = -2$, $\lambda = 1$, $\alpha = 0$, $\beta = -50$, $\delta = 50$, $r = 4$, $\kappa = -4$, and $\Delta\tau = 0.2$.

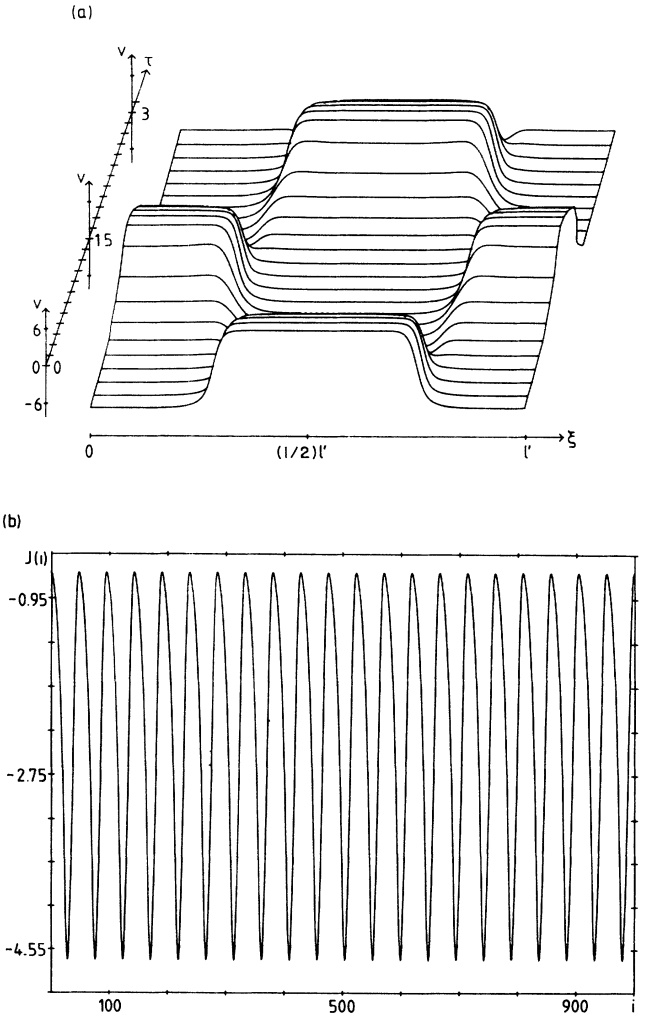

FIG. 11. (a) Time evolution of the spatial distribution of v and (b) time series J vs number i of time steps $\Delta\tau$ for oscillating homogeneous domains resulting from system (29) with $f(v)$ from (30). Parameters: $\sigma = 10$, $\mu = 0$, $\gamma = -0.02$, $\lambda = 1$, $\alpha = 0$, $\beta = -50$, $\delta = 5.2$, $r = 0.5$, $\kappa = -3$, and $\Delta\tau = 0.2$.

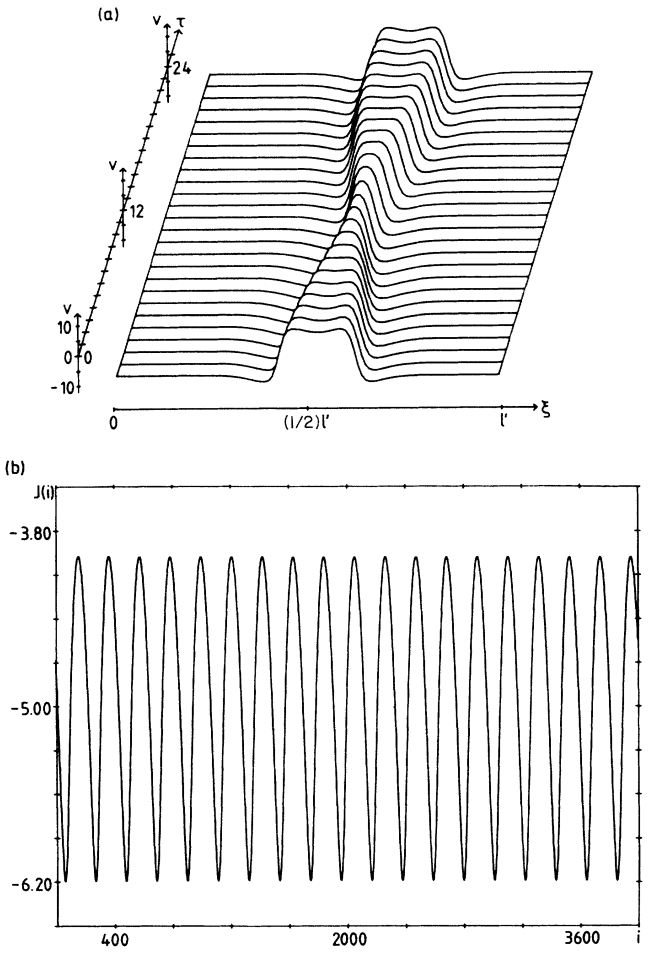

FIG. 12. (a) Time evolution of the spatial distribution of v and (b) time series J vs number i of time steps $\Delta\tau$ for a breathing filament obtained from system (28) with $f(v)$ from (30). Parameters: $\sigma=0.1$, $\mu=0$, $\gamma=-0.01$, $\lambda=1.37$, $\alpha=0$, $\beta=-50$, $\delta=5$, $r=0$, $\kappa=-0.5$, and $\Delta\tau=0.4$.

IV. APPLICATION OF THE MODEL TO REAL DEVICES

A. General requirements for appropriate devices

We have demonstrated that the model in the form of Eqs. (15a) and (15b) can be applied to real devices which have (a) the ability to define two zones of different electrical properties, where one of the zones must be resistive, while the other one must contain an S-shaped part in its j-E characteristic; and (b) two kinds of charge carriers which behave quasineutrally with respect to deviations from a reference state, i.e., changes in the concentration of charge carriers during the process of pattern formation must happen in pairs so that changing in the space-charge distribution can be neglected.

Many materials and devices show the effect that a lateral current density inhomogeneity is accompanied by a potential drop. Examples for this are p-i-n diodes.[16,18] Therefore it should be possible to identify two regions according to (a) in materials or devices which show this effect. The conditions described in point (b) are given in gas-discharge systems and double injection devices such as thyristorlike structures.[35] We believe that the model can be applied to the latter devices, too, although it is still an open problem to derive an equation of the form (11a) for them. In general, the experimental results observed at p-i-n diodes match the predictions of the model quite well.[18,36]

GaAs and Ge at low temperature are additional nonlinear materials that show stable inhomogeneous structures, that have a negative differential region in the $U(j)$ characteristic, and whose kinetics is dominated by impact ionization.[17,19] Although the behavior of these materials resembles the model, further detailed investigations are needed to decide whether these devices can be described with the current model. A detailed investigation with respect to the model of all the devices mentioned above is outstanding up to now and will be subject of future investigations.

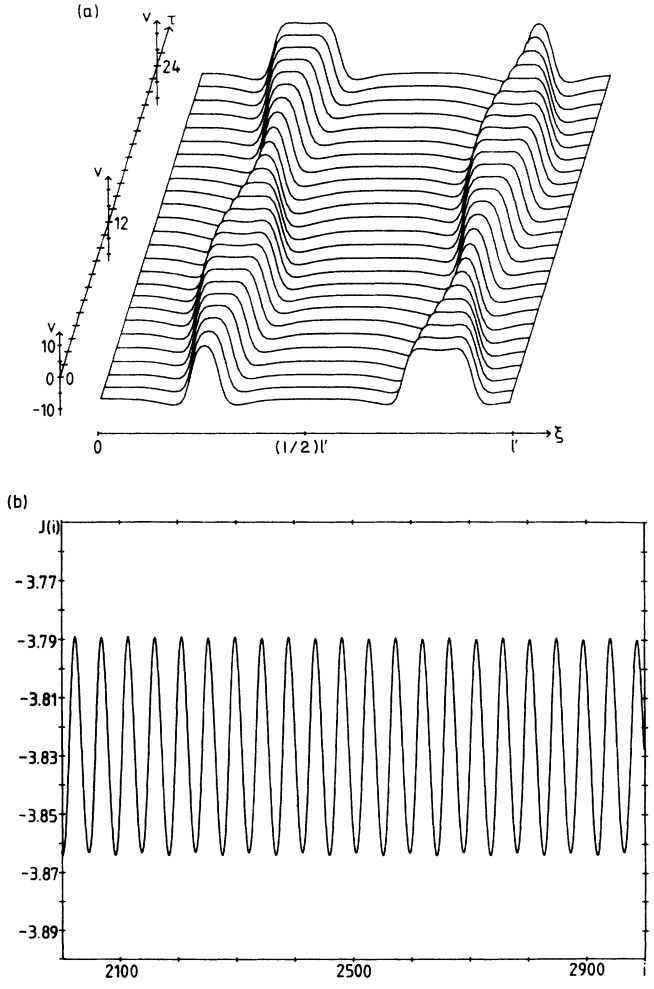

FIG. 13. (a) Time evolution of the spatial distribution of v and (b) time series J vs number i of time steps $\Delta\tau$ for the breathing of two filaments obtained from system (29) with $f(v)$ from (30). Parameters: $\sigma=0.1$, $\mu=0$, $\gamma=-0.01$, $\lambda=1.37$, $\alpha=0$, $\beta=-50$, $\delta=5$, $r=4$, $\kappa=-16$, and $\Delta\tau=0.4$.

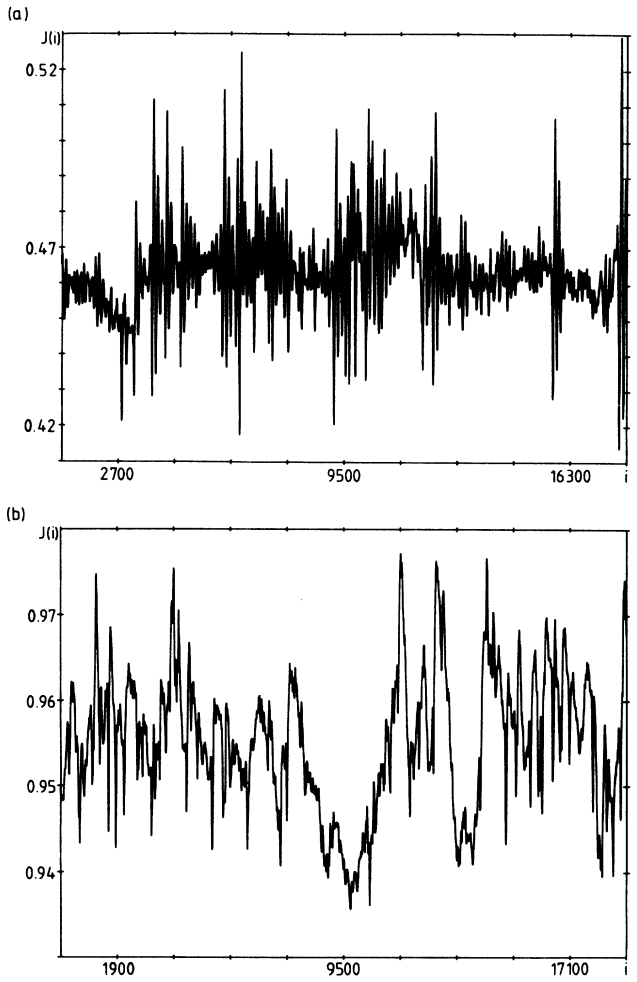

FIG. 14. Time series J vs number i of time steps $\Delta\tau$, in which the irregular behavior is caused by the drift term (a) for system (28) with $f(v)$ of (30); parameters: $\sigma=0.1$, $\mu=0.0005$, $\gamma=-11.5$, $\lambda=8$, $\alpha=0$, $\beta=0.6$, $\delta=0.1$, $r=7$, $\kappa=1$, and $\Delta\tau=0.02$; no noise; (b) for system (29) with $f(v)$ of (30); parameters: $\sigma=0.1$, $\mu=0.0003$, $\gamma=-11.5$, $\lambda=8$, $\alpha=0$, $\beta=0.6$, $\delta=1$, $r=10$, $\kappa=7.46$, and $\Delta\tau=0.01$; no noise.

B. Gas-discharge system—experimental setup and results

As mentioned above an application of the model is found in glow-discharge devices. Figure 15 shows schematically a cross section through a glow-discharge system parallel to the direction of the current flow. Volume ionization and processes at the cathode cause the generation of charge carriers and lead to transport processes that are associated to the typical distributions of charge carriers, electric field, space charges, etc. In this case, we have electrons and positive ions as charge carriers. The positive column of a discharge has a characteristic which contains a region of negative differential resistivity[30] and fulfills the requirement of quasineutrality.[29] From Fig. 15 it can be seen that the positive column has a positive net space charge. From these facts the positive column can serve as nonlinear layer in terms of the two-layer model.

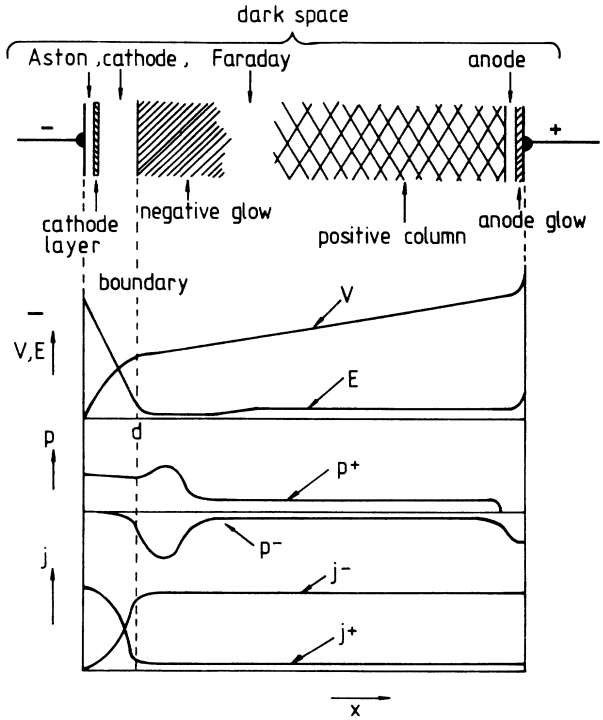

FIG. 15. Schematical spatial distribution of dark and luminous zones, space-charge density, electrical potential, and electric field in a glow-discharge system. It can be seen that the "net space charge" $e(n_0^+ - n_0^-)>0$ between the electrodes. (Cited from Ref. 33.)

In the following we describe the experimental setup and the results obtained with a gas-discharge system consisting of two rectangular electrodes, one of which is made of copper and the other of a doped silicon single crystal as resistive layer. The discharge slit between the electrodes is covered by glass plates, with a spacing of about 0.3 mm. The discharge slit contains an inert gas (He with 10% air) with a pressure varying in the range 10–160 hPa. This arrangement is connected to a voltage source through a series resistance R_S of about 80 kΩ. The device is shown in Fig. 16.

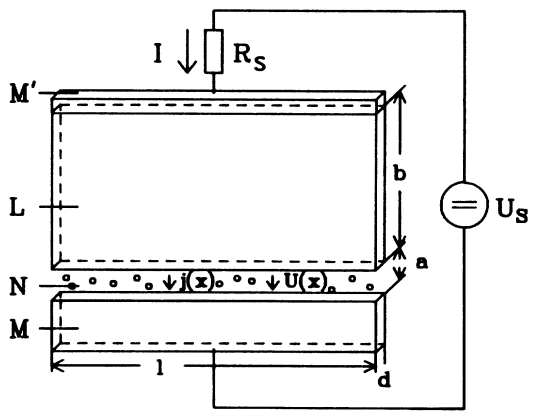

FIG. 16. Schematical arrangement of the gas-discharge system: M, Cu electrode; L, doped n or p silicon; M', Al contact of the layer L; N, gas-discharge gap; R_S, resistance; U_S, applied voltage.

In its dependence on the parameters pressure, applied voltage, and electrode distance, the gas-discharge system exhibits inhomogeneous patterns of the radiation density, which is proportional to the current density in a wide parameter range. In particular the following experiments have been performed.

By increasing the applied voltage U_S to a critical value, a luminous filament is spontaneously generated while the I-U_V characteristic exhibits a discontinuity. Further enhancement of U_S leads to a broadening of the filament and finally to its splitting into two filaments. Additional filaments result from subsequent division processes of the same kind. Figure 17(a) shows the evolution of the spatial distribution of the radiation density, which can be shown to be proportional to the current density in the investigated current-density range, when U_S is varied. The corresponding discontinuities in the global I-U_V characteristic are shown in Fig. 17(b).

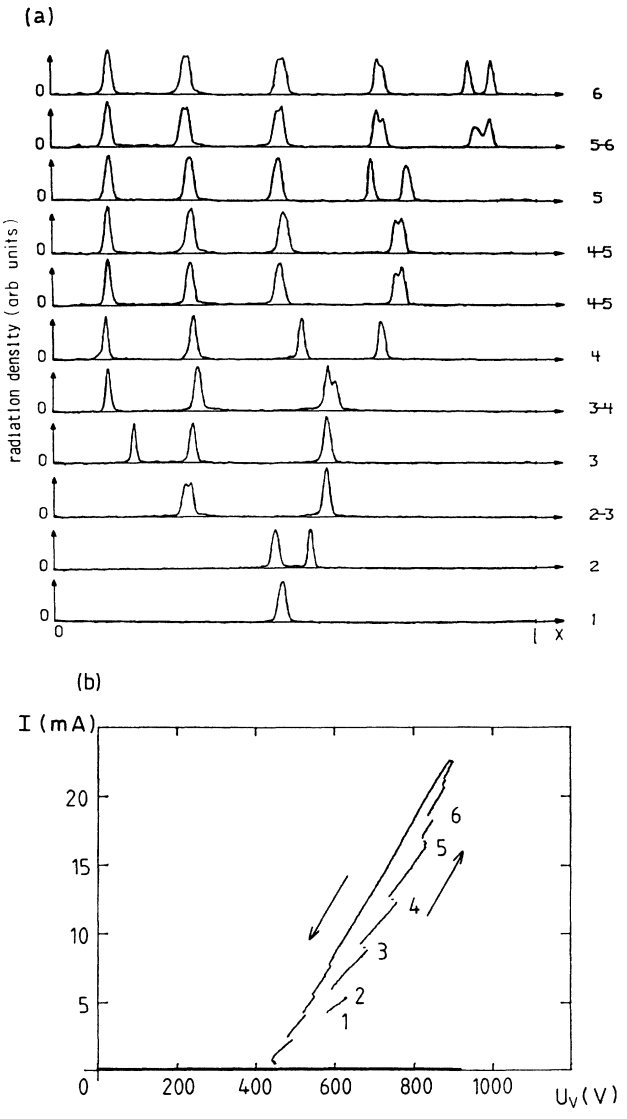

FIG. 17. (a) Spatial distribution of the radiation density, which is proportional to the current density and (b) corresponding I-U_V characteristic under variation of the externally applied voltage U_S. Parameters: specific resistivity, $\rho=0.9$ kΩ cm; pressure, 212 hPa; $R_S=74.5$ kΩ; $l=45$ mm; $d=0.3$ mm; $a=2.5$ mm; and $b=10$ mm.

By starting from a homogeneous discharge and decreasing the applied voltage, we obtain a spatially periodic pattern of the radiation density shown in Fig. 18. Furthermore, when the polarity of the applied voltage is changed, we observe a struggling motion of the filaments accompanied by an irregular behavior of the total current, which is shown in Fig. 19.

In order to determine the important parameters δ, σ, and μ for the experiments leading to stationary structures, further experiments have been done. The time τ that passes until the current density in the gas volume reaches its stationary value after an increase of the applied voltage was determined by means of a pulsed discharge between two metal electrodes. As result we obtain $\tau\approx10^{-6}$ s; from this we can estimate $\ell\approx5\times10^{-9}$ V s m^2/A (for details see Ref. 30). With $\epsilon_L\approx10$, $\epsilon_N\approx1$, and typical values $b\approx10$ mm, $\rho\approx0.9$ kΩ cm, and $a\approx3$ mm the gas-discharge system matches the case $\epsilon_L/b\gg\epsilon_N/a$ better than the case $\epsilon_L/b\ll E_N/a$, so that according to (18b), we obtain $\delta\approx0.14$ provided that $\chi\approx1$. From the intrinsic wave length, which appears in bifurcation experiments similar to that of Fig. 18, we can determine the ambipolar diffusion constant to $D_0\approx50$ cm^2/s, which is in a reasonable range between the diffusion constants of He ions and electrons, respectively. This leads to the value $\sigma\approx3\times10^{-5}$. Furthermore, we know that the positive column has a positive net space charge so that $\mu>0$ can be assumed.

These estimations reveal that the parameters for the experiments concerning the filament generation and the bifurcation from a homogeneous into a spatially periodic state lie in a suitable range. The conditions $\sigma,\delta<1$, which are decisive for the occurrence of stationary structures, and $\mu>0$, which is important for the division of filaments, are fulfilled. This gives us the legitimation to compare the experimental results to the numerical solutions in Sec. III.

Concerning the experiment in Fig. 17, the comparison to the numerical simulations of Eqs. (29) shows that the model with $\mu=0$ supplies the spontaneous generation of filaments and suffices to explain the occurrence of stable inhomogeneous current density distributions (see Fig. 8), but does not provide more details. The extended model with the appropriate $\mu\neq0$ matches the experimental results to a great extent. Numerical simulations and experimental observations are in good qualitative agreement about filament division [see Figs. 9(a) and 17(a)]. The theoretical J-T characteristic fits well the measured I-U_V characteristic in that the critical value of T for which the first filament is generated is larger than the value of T for which the division process starts [see Figs. 9(b) and 17(b)]. The experiment referring to Fig. 18 can be explained in terms of bifurcation theory in that the behavior of the radiation density is in good accordance with the predictions of Turing structures. A bifurcation analysis and a detailed comparison are the subjects of an additional paper,[30] where also a first quantitative analysis of the wavelength of the periodic patterns is given. To

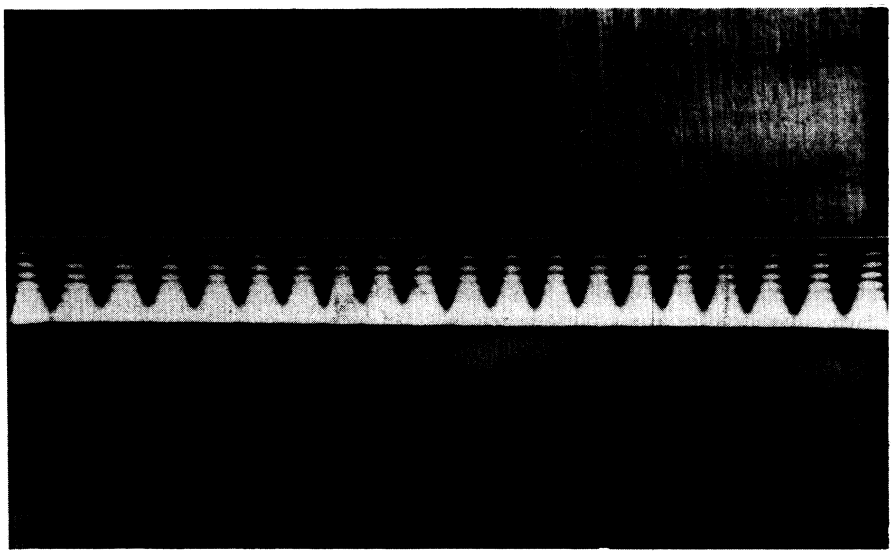

FIG. 18. Photograph of the spatially periodic structure of the luminous density in the discharge slit. Parameters: specific resistivity, $\rho=0.9$ kΩ cm; pressure, 90 hPa; $R_S=20$ kΩ; $l=45$ mm; $d=0.3$ mm; $a=4.6$ mm; $b=12$ mm, and $U_S=922$ V.

what extent the irregular behavior presented in Fig. 19 corresponds to the numerical results in Sec. III B upon mere qualitative agreement is still an open question.

In summary we can state that the experimental observations at the gas-discharge system are in good qualitative agreement with the numerical solutions of the model equations. Furthermore, the bifurcation experiments yield a first quantitative confirmation, whereas the filamentation up to now could not be calculated with exactly the value $\sigma\approx 3\times 10^{-5}$, which is typical for the gas-discharge system due to a present limitation of computing power.

As a variation of σ in the range 0.005–0.5 leads to similar results as described above for the case $\sigma=0.1$, we assume that a further decrease of σ would not effect a fundamental change in the behavior. From the present state of investigation we therefore conclude that the model can serve to reveal the mechanisms of pattern formation in the described gas-discharge system. Further work, especially concerning quantitative analyses, will be done to confirm the model.

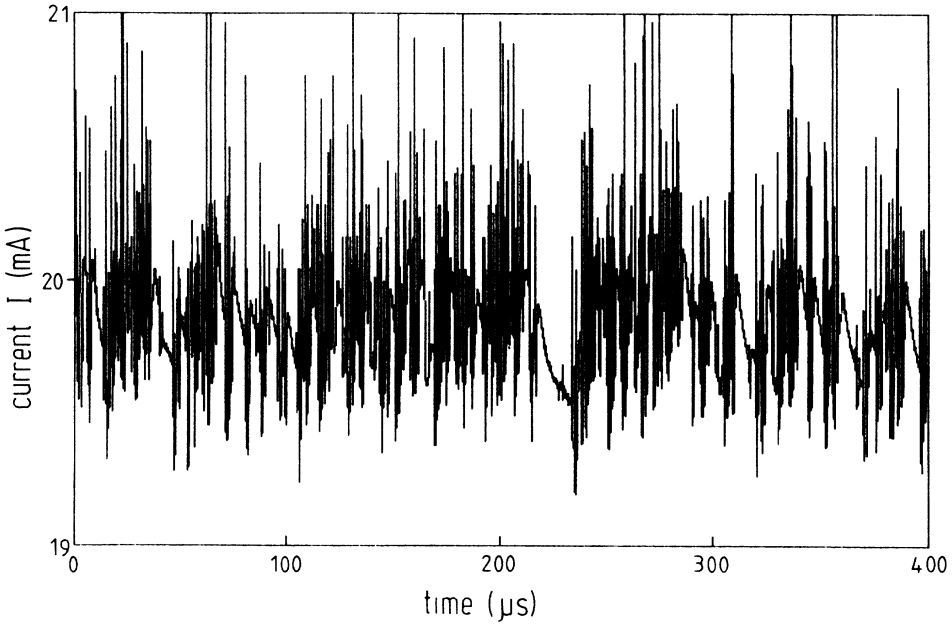

FIG. 19. Experimentally measured time series of irregular time-spatial behavior of the total current. Parameters: specific resistivity, $\rho=1.7$ kΩ cm; pressure, 230 hPa; $R_S=120$ kΩ, $l=45$ mm; $d=0.3$ mm; $a=2.5$ mm; $b=18$ mm; and $U_S=1250$ V.

V. CONCLUSIONS

We have derived, on a mesoscopic scale, a two-layer model for physical systems in which the reaction and transport of charge carriers causes the formation of patterns. The model consists of a pair of linear and nonlinear layers, each of which is described by a partial-differential equation. The approximation of the equation for the nonlinear layer is carried out for the case of two types of charge carriers whose densities deviate from a reference state but behave quasineutrally. By the quasineutrality the two equations for the charge carriers can be reduced to one and the space-charge terms drop out. The reference state itself can have a nonvanishing distribution of space charges, which is constant parallel to the electrodes. This is a typical situation for boundary layers in gas-discharge and in semiconductor devices. Therefore this should be a good approximation for systems such as, for example, capillary gas-discharge devices, *p-i-n* diodes and the thyristorlike devices.

The phenomenological equation for the nonlinear layer of Ref. 16 contains only a diffusion term and reaction term. Numerical simulations of the resulting system of equations show that this model supplies the spontaneous generation of filaments and roughly reflects the experimentally observed formation of inhomogeneous distributions of luminous density, and the I-U_V characteristic of the gas-discharge system described above. Drift effects caused by the net space charge and potential gradients at the interface of the two layers are taken into account in the so-far-developed extended model. The predictions of the extended model match the experimental results to a satisfactory extent, especially with respect to the division of filaments and the form of the global I-U_V characteristic.

Besides the comparison to experimental results, we have shown that the model possesses a rich variety of solutions depending on the values of parameters characterizing stationary and nonstationary states of the system. In particular we discussed spatially periodic solutions and the formation of filaments with special attention to some parameters and to the influence of the drift term. We have studied the dynamic behavior of breathing filaments, nervelike pulses and irregular motion.

Further investigations will be concerned with an analysis of the quantitative agreements between experimental and theoretical results. For this purpose, we must determine carefully the parameters corresponding to the material constants, and the j-E characteristic of the gas-discharge system. Another matter of interest is to find out to what extent the dynamic behavior of the model corresponds to the experimental observations. This includes the dynamics of filament division and the experimentally observed irregular behavior of the luminous density distribution. We hope that the model can be applied also to the two-dimensional high-frequency gas-discharge system of the Boyers-Tiller type.[15]

The next step in the further development of the model will include extensions in modeling the nonlinear layer for thyristorlike devices and models for the nonlinear layer in which the condition of quasineutrality is not fulfilled. In the latter case we have to deal with stronger inner fields because of the charge separation. As a result the internal drift terms can no longer be disregarded compared to the external drift terms, which are proportional to $U_{,x}$. A typical example for effects of this type is the injection of one kind of charge carrier in semiconductor devices.

ACKNOWLEDGMENTS

The authors appreciate Professor J. Pankove's helpful discussions. They also would like to thank M. Pohlmann for his support in the numerical calculations.

APPENDIX A

Using the definitions (2) we get from (1a)

$$n_{1,t}^{-}=f+\mu_x^{-}n_{1,x}^{-}E_{1x}+\mu_x^{-}n^{-}E_{1x,x}+\mu_z^{-}n_{,z}^{-}E_z+\mu_z^{-}n^{-}E_{z,z}+D_x^{-}n_{1,xx}^{-}+D_z^{-}n_{,zz}^{-}$$

and the corresponding equation for the positive charge carriers. The Poisson equation turns to

$$E_{1x,x}+E_{0z,z}+E_{1z,z}=(e/\epsilon\epsilon_0)(n_0^{+}+n_1^{+}-n_0^{-}-n_1^{-}+C)=(e/\epsilon\epsilon_0)(n_0^{+}-n_0^{-}+C)=E_{0z,z}\ .$$

Summing up in F all terms containing no operators in x and/or t we obtain

$$n_{1,t}^{-}=F^{-}+\mu_x^{-}n_{1,x}^{-}E_{1x}+\mu_x^{-}n^{-}E_{1x,x}+D_x^{-}n_{1,xx}^{-}\mu_x^{+}n^{+}\ , \tag{A1}$$

$$n_{1,t}^{+}=F^{+}-\mu_x^{+}n_{1,x}^{+}E_{1x}-\mu_x^{+}n^{+}E_{1x,x}+D_x^{+}n_{1,xx}^{+}\mu_x^{-}n^{-}\ ,$$

with the "effective reaction terms" F^{+} and F^{-} given by

$$F^{-}=f+\mu_z^{-}n_{,z}^{-}E_z+\mu_z^{-}n^{-}E_{z,z}+D_z^{-}n_{,zz}^{-}\ ,$$

$$F^{+}=f-\mu_z^{+}n_{,z}^{+}E_z-\mu_z^{+}n^{+}E_{z,z}+D_z^{+}n_{,zz}^{+}\ ,$$

and $F^{-}=F^{+}=0$ for $P_0=(n_0^{-},n_0^{+},\mathrm{E}_0)$ according to (2b). Note that F^{-} and F^{+} contain z derivations and are therefore operators.

Multiplication by the factors $\mu_x^{+}n^{+}$ and $\mu_x^{-}n^{-}$, respectively, and adding both equations (A1) causes the space charge terms $\mu_x^{-}n^{-}E_{1x,x}$ and $-\mu_x^{+}n^{+}E_{1x,x}$ to drop out. With $n_1=n_1^{-}\approx n_1^{+}$ it follows that

$$n_{1,t}=F^{*}(n_0^{+}+n_1,n_0^{-}+n_1,E_{0z}+E_{1z})+\mu^{*}n_{1,x}E_{1x}+D^{*}n_{1,xx}\ , \tag{A2a}$$

with

$$\mu^*=\frac{\mu_x^+\mu_x^-(n_0^+-n_0^-)}{\mu_x^+n^++\mu_x^-n^-}=\frac{\mu_x^+\mu_x^-(n_0^+-n_0^-)}{\mu_x^+n_0^++\mu_x^-n_0^-}+\mathcal{T}$$
$$=\mu_0^*+\mathcal{T}\ ,$$
$$D^*=\frac{\mu_x^+D_x^-n^++D_x^+\mu_x^-n^-}{\mu_x^+n^++\mu_x^-n^-}$$
$$=\frac{\mu_x^+D_x^-n_0^++D_x^+\mu_x^-n_0^-}{\mu_x^+n_0^++\mu_x^-n_0^-}+\mathcal{T}$$
$$=D_0^*+\mathcal{T}\ ,$$
$$F^*=\frac{\mu_x^+n^+F^-+\mu_x^-n^-F^+}{\mu_x^+n^++\mu_x^-n^-}\ ,$$
$$=D_0^*+\mathcal{T}\ ,$$
$$F^*=\frac{\mu_x^+n^+F^-+\mu_x^-n^-F^+}{\mu_x^+n^++\mu_x^-n^-}\ ,$$

where $\mathcal{T}$ represent terms higher than first order in n_1.

Expressing F^* in terms of the deviations we define the function $G_0^*(n_1,E_{1z},z)=F^*$ with coefficients that depend on the reference state. Approximating μ^* and D^* by their constant parts μ_0^* and D_0^* and introducing G_0^* we get from Eq. (A2a)

$$n_{1,t}=G_0^*(n_1,E_{1z})+\mu_0^*n_{1,x}E_{1x}+D_0^*n_{1,xx}\ . \quad \text{(A2b)}$$

Note that this equation is z dependent.

The z component of the current density j is given by

$$j_z=j_z^-+j_z^+$$
$$=-e(n_0^-+n_1)(v_{0z}^-+v_{1z}^-)+e(n_0^++n_1)(v_{0z}^++v_{1z}^+)$$
$$=-e(n_0^-v_{0z}^-+n_0^-v_{1z}^-+n_1v_{0z}^-+n_1v_{1z}^-$$
$$-n_0^+v_{0z}^+-n_0^+v_{1z}^+-n_1v_{0z}^+-n_1v_{1z}^+)\ .$$

With $v_z^+=\mu^+E_z=\alpha\mu^-E_z=-\alpha v_z^-$ we get

$$j_z=-e(n_0^-v_{0z}^-+n_0^-v_{1z}^-+n_1v_{0z}^-+n_1v_{1z}^-$$
$$+\alpha n_0^+v_{0z}^-+\alpha n_0^+v_{1z}^-+\alpha n_1v_{0z}^-+\alpha n_1v_{1z}^-)$$
$$=j_0+j_{01}+j_{10}+j_2$$
$$=j_0+j_{Nz}\ , \quad \text{(A3)}$$

with

$$j_0=-e(n_0^-+n_0^+\alpha)v_{0z}^-=a_0E_{0z}\ ,$$
$$a_0=-e(n_0^-+n_0^+\alpha)\mu_z^-$$
$$j_{01}=-e(n_0^-+n_0^+\alpha)v_{1z}^-=a_0E_{1z}=a_0E_{Nz}\ ,$$
$$j_{10}=-e(1+\alpha)n_1v_{0z}^-=a_2n_1E_{0z},\quad a_2=-e(1+\alpha)\mu_z^-$$
$$j_2=-e(1+\alpha)n_1v_{1z}^-=j_{10}E_{1z}/E_{0z}\ ,$$
$$j_{Nz}=j_{01}+j_{10}+j_2\ .$$

Multiplying (A2b) by $-e(1+\alpha)v_{0z}^-$ we obtain an evolution equation for the partial current density j_{10},

$$j_{10,t}=-e(1+\alpha)v_{0z}^-n_{1,t}$$
$$=-e(1+\alpha)v_{0z}^-G_0^*-\mu_0^*e(1+\alpha)v_{0z}^-n_{1,x}E_{1x}$$
$$-D_0^*e(1+\alpha)v_{0z}^-n_{1,xx}$$
$$=G_0+\mu_0^*j_{10,x}E_{1x}+D_0^*j_{10,xx}\ , \quad \text{(A4)}$$

with G_0 defined as

$$G_0(j_{10}(x,z),E_{1z}(x,z))$$
$$=-e(1+\alpha)v_{0z}^-G_0^*(n_1,E_{1z})$$
$$=-e(1+\alpha)v_{0z}^-G_0^*(j_{10}/[-e(1+\alpha)\mu_z^-E_{0z}],E_{1z})$$

and $G_0(0,0)=0$ because of $F^-=F^+=0$ for $n_1^-=n_1^+=0$.

APPENDIX B

Denoting the deviation from a mean value $\langle Y\rangle$ by ∂Y we can write every quantity as $Y=\langle Y\rangle+\partial Y$. Inserting Eq. (8), the expansion of G_0, in Eq. (6), and splitting the quantities we get

$$\langle j_{10}\rangle_{,t}+\partial j_{10,t}=(\langle\mu_0^*\rangle+\partial\mu)(\langle j_{10}\rangle_{,x}+\partial j_{10,x})(\langle E_{1x}\rangle+\partial E_{1x})+(\langle D_0^*\rangle+\partial D)(\langle j_{10}\rangle_{,xx}+\partial j_{10,xx})$$
$$+(\langle G_j\rangle+\partial G_j)(\langle j_{10}\rangle+\partial j_{10})+(\langle G_E\rangle+\partial G_E)(\langle E_{1z}\rangle+\partial E_{1z})$$
$$+(\langle G_{jE}\rangle+\partial G_{jE})(\langle j_{10}\rangle+\partial j_{10})(\langle E_{1z}\rangle+\partial E_{1z})$$
$$+(\langle G_{jj}\rangle+\partial G_{jj})(\langle j_{10}\rangle+\partial j_{10})^2+(\langle G_{EE}\rangle+\partial G_{EE})(\langle E_{1z}\rangle+\partial E_{1z})^2+\cdots\ .$$

Averaging this equation yields

$$
\begin{aligned}
\langle j_{10}\rangle_{,t} &= \langle \mu_0^*\rangle\langle j_{10}\rangle_{,x}\langle E_{1x}\rangle + \langle D_0^*\rangle\langle j_{10}\rangle_{,xx} + \langle G_j\rangle\langle j_{10}\rangle + \langle G_E\rangle\langle E_{1z}\rangle + \langle G_{jE}\rangle\langle j_{10}\rangle\langle E_{1z}\rangle + \cdots \\
&\quad + \langle \partial\mu\partial j_{10,x}\rangle\langle E_{1x}\rangle + \langle \partial\mu\partial E_{1x}\rangle\langle j_{10}\rangle_{,x} + \langle \partial j_{10}\partial E_{1x}\rangle\langle \mu_0^*\rangle + \langle \partial\mu\partial j_{10}\partial E_{1x}\rangle + \langle \partial D\partial j_{10,xx}\rangle \\
&\quad + \langle \partial G_j\partial j_{10}\rangle + \langle \partial G_E\partial E_{1z}\rangle + \langle \partial G_{jE}\partial j_{10}\rangle\langle E_{1z}\rangle \\
&\quad + \langle \partial j_{10}\partial E_{1z}\rangle\langle G_{jE}\rangle + \langle \partial G_{jE}\partial E_{1z}\rangle\langle j_{10}\rangle + \langle \partial G_{jE}\partial j_{10}\partial E_{1z}\rangle + \cdots \\
&= \langle \mu_0^*\rangle\langle j_{10}\rangle_{,x}\langle E_{1x}\rangle + \langle D_0^*\rangle\langle j_{10}\rangle_{,xx} + \langle G_j\rangle\langle j_{10}\rangle + \langle G_E\rangle\langle E_{1z}\rangle + \langle G_{jE}\rangle\langle j_{10}\rangle\langle E_{1z}\rangle + \cdots + R_m \\
&= \langle \mu_0^*\rangle\langle j_{10}\rangle_{,x}\langle E_{1x}\rangle + \langle D_0^*\rangle\langle j_{10}\rangle_{,xx} + \langle G_0\rangle(\langle j_{10}\rangle,\langle E_{1z}\rangle) + R_m \ ,
\end{aligned}
$$

where R_m contains all terms containing mean values of higher-order products of ∂Y_j.

---

*Present address: Center for Optoelectronic Computing Systems and Department of Electrical and Computer Engineering, University of Colorado, Boulder, CO 80309-0425.

[1] G. Nicolis and I. Prigogine, *Self-Organization in Non-Equilibrium Systems* (Wiley, New York, 1981).

[2] B. P. Belousov, Sb. Ref. Radats. Med. Moscow 145 (1958).

[3] A. M. Zhabotinsky and A. N. Zaikin, J. Theor. Biol. **40**, 45 (1973).

[4] *Oscillations and Traveling Waves in Chemical Systems,* edited by R. J. Field and M. Burger (Wiley, New York, 1985).

[5] A. Gierer and M. Meinhardt, Lect. Math. Life Sciences **7**, 163 (1974).

[6] J. D. Murray, J. Theor. Biol. **88**, 161 (1981).

[7] F. Rothe, J. Math. Biol. **7**, 375 (1979).

[8] K. Maginu, Math. Biosci. **27**, 17 (1975).

[9] C. Radehaus, Ph.D. thesis, University of Münster, 1987.

[10] B. S. Kerner and V. V. Osipov, Zh. Eksp. Teor. Fiz. **79**, 2218 (1980) [Sov. Phys.—JETP **52**, 1122 (1980)].

[11] H.-G. Purwins, G. Klempt, and J. Berkemeier, Festkörperprobleme **27**, 27 (1987).

[12] C. Radehaus, T. Dirksmeyer, H. Willebrand, and H.-G. Purwins, Phys. Lett. A **125**, 92 (1987).

[13] K. G. Müller, Phys. Rev. A **37**, 4836 (1988).

[14] Yu. A. Astrov and L. M. Portsel, Zh. Tekh. Fiz. **51**, 2502 (1981) [Sov. Phys.—Tech. Phys. **26**, 1480 (1981)]

[15] D. G. Boyers and W. A. Tiller, Appl. Phys. Lett. **41**, 28 (1982).

[16] C. Radehaus, K. Kardell, H. Baumann, D. Jäger, and H.-G. Purwins, Z. Phys. B **65**, 515 (1987).

[17] K. M. Mayer, J. Peinke, B. Röhricht, J. Parisi, and R. P. Heubener, Phys. Scr. **T19**, 505 (1987).

[18] H. Baumann, R. Symanczyk, C. Radehaus, H.-G. Purwins, and D. Jäger, Phys. Lett. A **123**, 421 (1987).

[19] U. Rau, J. Peinke, J. Parisi, and R. P. Huebener, Z. Phys. B **71**, 305 (1988).

[20] E. Schöll, *Nonequilibrium Phase Transitions in Semiconductors* (Springer, Berlin, 1987).

[21] B. S. Kerner and V. F. Sinkevich, Pis'ma Zh. Eksp. Teor. Fiz. **36**, 359 (1982) [JETP Lett. **36**, 436 (1982)].

[22] Yu. I. Balkarei, M. G. Evtikhov, and M. I. Elinson, Zh. Tekh. Fiz. **57**, 209 (1987) [Sov. Phys.—Tech. Phys. **32**, 127 (1987)].

[23] K. Kardell, C. Radehaus, R. Dohmen, and H.-G. Purwins, J. Appl. Phys. **64**, 6336 (1988).

[24] H.-G. Purwins, C. Radehaus, and J. Berkemeier, Z. Naturforsch. **43A**, 17 (1988).

[25] H.-G. Purwins and C. Radehaus, in *Neural and Synergetic Computer,* Vol. 42 of *Springer Series in Synergetics,* edited by H. Haken (Springer, Berlin, 1988).

[26] T. Dirksmeyer, Ph.D. thesis, University of Münster, 1989.

[27] S. Selberherr, *Analysis and Simulation of Semiconductor Devices* (Springer-Verlag, New York, 1984).

[28] E. Schöll, in *Proceedings of the 19th International Conference on the Physics of Semiconductors,* edited by M. Grynberg (Polish Academy of Sciences, Warsaw, 1988).

[29] D. B. Graves and K. F. Jensen, IEEE Trans. Plasma Sci. **PS-14**, 78 (1986).

[30] C. Radehaus, H. Willebrand, R. Dohmen, F.-J. Niedernostheide, G. Bengel, and H.-G. Purwins, J. Appl. Phys. (to be published).

[31] J. Berkemeier, T. Dirksmeyer, G. Klempt, and H.-G. Purwins, Z. Phys. B **65**, 255 (1986).

[32] M. Mimura (private communication).

[33] A. von Engel, *Ionized Gases* (Oxford University Press, New York, 1965).

[34] There is a large amount of literature closely related to our work; see, e.g., H. Fujii, M. Mimura, and Y. Nishiura, Physica D **5**, 1 (1982); V. V. Gafilchuk, B. S. Kerner, V. V. Osipov, and A. G. Yuzhanin, Fiz. Tekh. Poluprovodn. **22**, 2051 (1988) [Sov. Phys.—Semicond. **22**, 1298 (1988)]; B. S. Kerner and V. V. Osipov, in *Self-Organization by Nonlinear Irreversible Processes,* Vol. 33 of *Springer Series in Synergetics,* edited by W. Ebeling and H. Ullbricht (Springer-Verlag, Berlin, 1986); P. C. Fife, J. Chem. Phys. **64**, 554 (1976); in *Nonlinear Problems: Present and Future,* edited by A. R. Bishop, D. K. Campbell, and B. Nicolaenko (North-Holland, Amsterdam, 1982); J. Nagumo, S. Arimoto, and S. Yoshizawa, Proc. IRE **50**, 500 (1962); K. Maginu, Math. Biosci. **27**, 17 (1975); F. Rothe, *ibid.* **7**, 375 (1979).

[35] J. Pankove, R. Hayes, A. Mayerfeld, M. Hanna, G. Oh, D. Szmyd, D. Suda, S. Asher, R. Matson, J. Arent, G. Borghs, and M. Harvey, SPIE Trans. **963**, 191 (1988).

[36] H. Baumann, Ph.D. thesis, University of Münster, 1988.

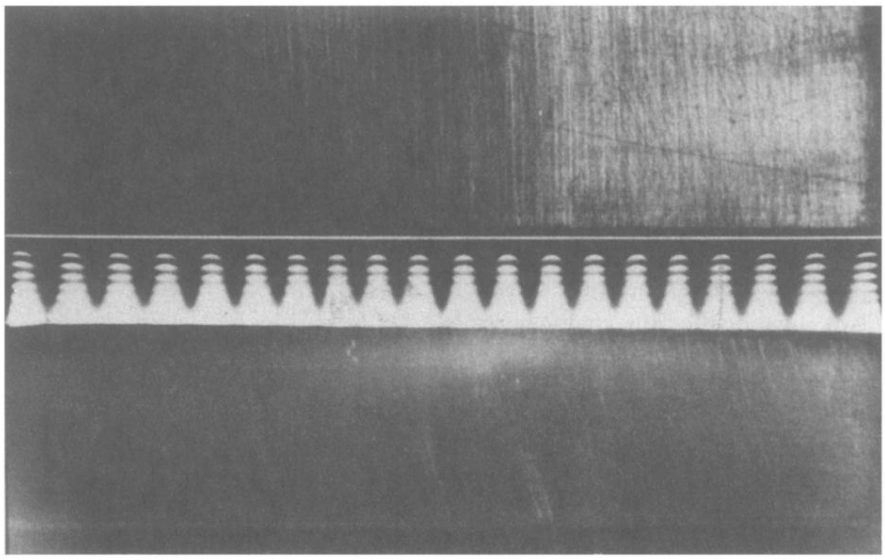

FIG. 18. Photograph of the spatially periodic structure of the luminous density in the discharge slit. Parameters: specific resistivity, $\rho = 0.9$ kΩ cm; pressure, 90 hPa; $R_S = 20$ kΩ; $l = 45$ mm; $d = 0.3$ mm; $a = 4.6$ mm; $b = 12$ mm, and $U_S = 922$ V.